6-25-2013

Alternative Plasmonic Materials: Beyond Gold and Silver

Gururaj V. Naik
Birck Nanotechnology Center, Purdue University, gnaik@purdue.edu

Vladimir M. Shalaev
Birck Nanotechnology Center, Purdue University, shalaev@purdue.edu

Alexandra Boltasseva
Birck Nanotechnology Center, Purdue University, aeb@purdue.edu

Naik, Gururaj V.; Shalaev, Vladimir M.; and Boltasseva, Alexandra, "Alternative Plasmonic Materials: Beyond Gold and Silver" (2013). *Birck and NCN Publications.* Paper 1422.
http://dx.doi.org/10.1002/adma.201205076

Alternative Plasmonic Materials: Beyond Gold and Silver

*Gururaj V. Naik, Vladimir M. Shalaev, and Alexandra Boltasseva**

Materials research plays a vital role in transforming breakthrough scientific ideas into next-generation technology. Similar to the way silicon revolutionized the microelectronics industry, the proper materials can greatly impact the field of plasmonics and metamaterials. Currently, research in plasmonics and metamaterials lacks good material building blocks in order to realize useful devices. Such devices suffer from many drawbacks arising from the undesirable properties of their material building blocks, especially metals. There are many materials, other than conventional metallic components such as gold and silver, that exhibit metallic properties and provide advantages in device performance, design flexibility, fabrication, integration, and tunability. This review explores different material classes for plasmonic and metamaterial applications, such as conventional semiconductors, transparent conducting oxides, perovskite oxides, metal nitrides, silicides, germanides, and 2D materials such as graphene. This review provides a summary of the recent developments in the search for better plasmonic materials and an outlook of further research directions.

1. Introduction

The development of materials technology has been an important part of human history for many ages. Materials technology enables novel applications, and they in turn assist in the exploration of new science. New scientific concepts enable even more advanced materials technologies; the progress in metallurgy from the Bronze Age to the Iron Age is a prime example of this advancement. Materials play an important role in the positive feedback loop established between science and technology. Two of the most ubiquitous examples from the past century are those of semiconductor technologies and optical communications. Both of these areas have revolutionized our capability to process information, and the speeds at which we can process information have risen exponentially in the past few decades, mainly because of the scaling of semiconductor electronic components predicted by Moore's Law.[1] The elementary electronic switch (the transistor) has been scaled down from about 200 nm to 35 nm within the last decade to achieve drastically higher operating speeds. Further significant scaling, however, poses many substantial difficulties such as short-channel effects, gate leakage and drastically increasing power density.[2,3] As a result of these challenges, alternative technologies have gained significant attention in the quest to increase information processing speeds. As one such alternative technology, the field of plasmonics has the potential to support our ever-increasing needs for information processing.[4] Recently, the application domain of plasmonics has expanded significantly with the introduction of the related fields of metamaterials[5–6] and transformation optics (TO).[7] Many novel physical phenomena and application prototypes have been demonstrated so far in plasmonics, metamaterials and TO. However, advancing these novel concepts and prototypes into real, practical technologies requires support from materials technology.[8–10] Plasmonics and metamaterials are in a situation where engineering the properties of the constituent materials is of utmost importance.[8] In this review we consider the recent developments in the emerging field of materials research for plasmonics and metamaterials. Specially, we focus on the design of metal-like materials using unconventional materials, and we discuss their advantages and disadvantages in various applications for plasmonics and metamaterials. Before we discuss the details of the problems arising from conventional plasmonic materials and how to overcome these issues with new materials, it is important to understand how plasmonic and metamaterial devices work and the role of plasmonic materials in those devices. We therefore begin with an overview of plasmonic and metamaterial devices as a motivation for the need for new metal-like materials.

G. V. Naik, Prof. V. M. Shalaev, Prof. A. Boltasseva
School of Electrical & Computer Engineering
and Birck Nanotechnology Center
Purdue University
1205 West State Street, West Lafayette
IN 47907-2057, USA
E-mail: aeb@purdue.edu
Prof. V. M. Shalaev
The Russian Quantum Center
Novaya Str., 100, BC "URAL", Skolkovo, Moscow region, 143025, Russia
Prof. A. Boltasseva
DTU Fotonik
Technical University of Denmark
Ørsteds Plads 343, DK-2800, Kgs. Lyngby, Denmark

DOI: 10.1002/adma.201205076

2. Motivation

The field of plasmonics has received significant attention recently, although some applications of plasmonics have been known for ages.[11–14] The Lycurgus Cup of the ancient Roman era and the stained glass decorating medieval cathedrals both get their vibrant colors from optical plasmonic

resonances induced in the metal nanoparticles embedded in the glass.[12] When light interacts with a metal, the cloud of free electrons in the metal can support a wave of charge density fluctuations on the surface of the metal.[15] This phenomenon is called a surface plasmon wave and can be used in a number of advanced applications. Surface plasmons can couple light strongly to the metal surface and thereby greatly enhance light-matter interactions. These strong interactions have two important consequences, light can be confined in an area smaller than that predicted by the diffraction limit; and the local electromagnetic field intensity can be enhanced by many orders of magnitude. These consequences are of special importance because they open a horizon of new physical phenomena whose applications could revolutionize our daily lives. One of the major applications of plasmonics is in chemical sensing.[16] Since plasmonics enhance light-matter interactions by many orders of magnitude, minute changes in the local environment can be amplified significantly to enable ultrasensitive detection. Yet another important possible application of plasmonics is in information processing.[4,14] The need for new technologies to enable higher processing speeds is growing due to the difficulty in scaling nanoelectronic components. Optical communication is the fastest available means of information processing because of its extremely high bandwidth. However, optical components are relatively bulky and cannot be packed together as compactly as the ubiquitous nanoelectronic components. For example, each integrated circuit chip consists of billions of tiny transistors, each only a few tens of nanometers in size. Such high-density packing is not possible for optical components because of the diffraction limit. In conventional optical systems, light can only be focused to a size on the order of the wavelength due to diffraction effects. At the telecommunications wavelength of 1.55 micrometers, for example, the diffraction limit for light in a high-index dielectric such as silicon is about 500 nm. Thus, the sizes of optical components must be at least a few hundreds of nanometers in size to avoid diffraction. Further size reductions below the diffraction limit are possible with plasmonics (see **Figure 1**a). With the help of plasmonics, we can miniaturize optical components and integrate them on-chip while leveraging on the large bandwidth of light.

Manipulating light at the nanoscale using plasmonics is complemented by metamaterials and TO. Transformation optics is a concept that enables extreme control over the flow of light.[7,17,18] This control often requires a certain distribution of permittivity and permeability within the material. Since natural materials cannot provide such arbitrary distributions in material's optical properties, artificial materials called metamaterials are used instead. Metamaterials are artificial materials whose properties are engineered by design.[19] The building elements of a metamaterial (called meta-molecules or meta-atoms) are much smaller than the wavelength, unlike the building blocks of photonic crystals that have sizes on the order of the wavelength (see Figure 1b). The careful design of meta-molecules is critical for achieving the desired optical characteristics of a metamaterial. New functionalities such as optical magnetism, sub-diffraction resolution and a negative refractive index have been demonstrated based on the principles of metamaterials and TO.[5]

Gururaj V. Naik is a PhD student in the school of Electrical & Computer Engineering at Purdue University. He specializes in nanophotonics, plasmonics & metamaterials, materials and nanofabrication. He has been a recipient of many awards including the Outstanding Graduate Student Research Award from College of Engineering, Purdue University and Gold Medal from the Indian Institute of Science, Bangalore. Gururaj Naik is a member of SPIE, OSA, and IEEE and serves as a Graduate Ambassador of Birck Nanotechnology Center at Purdue University.

Vladimir M. Shalaev, Scientific Director for Nanophotonics in Birck Nanotechnology Center and Distinguished Professor of Electrical and Computer Engineering at Purdue University, specializes in nanophotonics, plasmonics, and optical metamaterials. Vlad Shalaev received several awards for his research in the field of nanophotonics and metamaterials, including the Max Born Award of the Optical Society of America for his pioneering contributions to the field of optical metamaterials and the Willis E. Lamb Award for Laser Science and Quantum Optics. He is a Fellow of IEEE, APS, SPIE, and OSA.

Alexandra Boltasseva (Ph.D. in Electrical Engineering, 2004) is an Assistant Professor at the School of Electrical and Computer Engineering and Birck Nanotechnology Center, Purdue University, and an adjunct Associate Professor at Technical University of Denmark (DTU). Alexandra specializes in nanophotonics, nanofabrication, plasmonics, and metamaterials. She has received many awards including MRS Outstanding Young Investigator Award, IEEE Photonics Society Young Investigator Award, MIT Technology Review Top Young Innovator (TR35) award, and the Purdue College of Engineering Early Career Research Award. She is topical editor for Optics Letters, a senior member of the OSA, and a member of the IEEE, SPIE, and MRS.

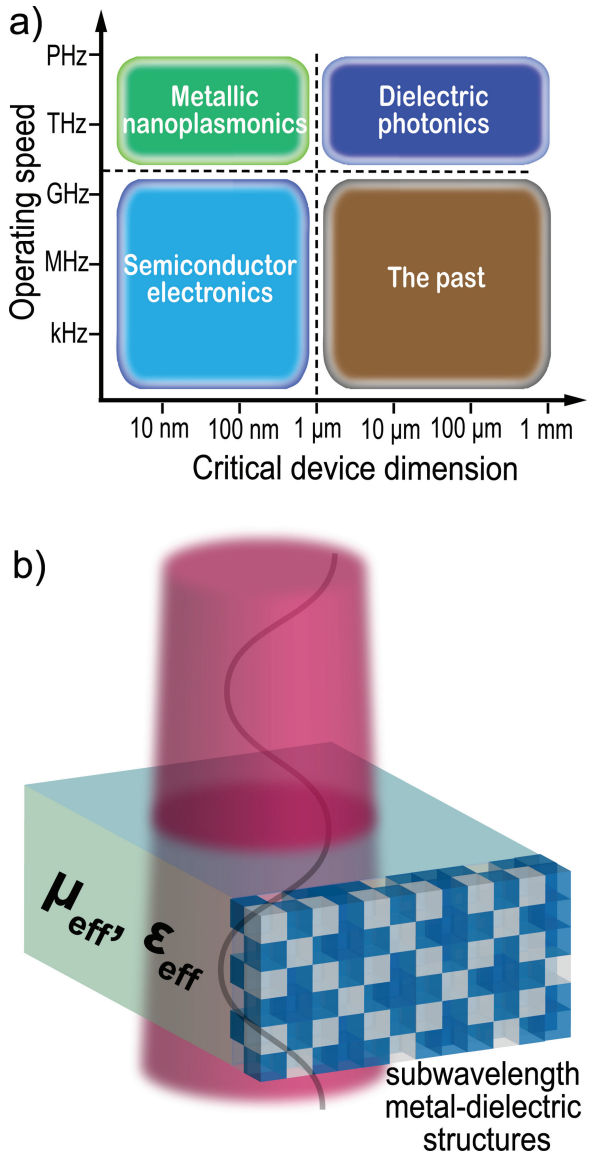

Figure 1. a) Our information processing demands are met by various technologies offering different trade-offs between the integration density or device dimension and the speed of processing (redrawn from ref.[4]). b) A metamaterial made from subwavelength metal-dielectric inclusions exhibits effective permeability and permittivity that natural materials may not be able to exhibit.

Metamaterials are built from natural materials that are patterned at the nanoscale and arranged in a specific geometry. In general, the constituents of a meta-molecule are metals and dielectrics. Metals are also called the plasmonic elements of a metamaterial because of the nature of their interaction with light. The optical response of these natural materials is described by their dielectric permittivity, ε, and magnetic permeability, μ.[20] At optical frequencies, the magnetic interaction is weak and, hence, permeability is very close to one for all natural materials. Therefore dielectric permittivity (also known as the dielectric function) is the parameter that describes the optical response of natural materials. Permittivity is a complex quantity whose real part (ε' or ε_1) signifies the polarization response and whose imaginary part (ε'' or ε_2) denotes the optical losses. At optical frequencies, metals exhibit a negative real permittivity, while dielectrics exhibit a positive real permittivity.[21] The imaginary part of the permittivity for dielectrics can be practically zero, but this is not the case for metals–metals are always associated with losses that arise largely from electronic transitions. Loss is a critical factor that limits the performance of optical devices. There are other issues associated with using metals in real applications, which forms a bottleneck in the design, fabrication and integration of various plasmonic and metamaterial devices. In the following section, we provide an overview of the important drawbacks associated with conventional plasmonic materials.

3. Problems with Conventional Plasmonic Materials

Metals such as gold and silver are commonly used in plasmonic and optical metamaterial devices because of their small ohmic losses or high DC conductivity. However, at optical frequencies another loss mechanism namely interband transitions plays an important role in these metals.[22] Loss arising from interband transitions occurs when a valence electron in a metal absorbs a photon to jump to the Fermi surface or an electron near the Fermi-surface absorbs a photon to jump to the next unoccupied conduction band.[23] This is the loss mechanism that is responsible for the color of copper and gold. **Figure 2** shows the imaginary part of permittivity of gold in the optical range adopted from Johnson & Christy.[22] The loss depicted by the imaginary part of permittivity can be split into two parts: interband and intraband losses. The intraband losses (or Drude losses) in gold are high in the near-infrared (NIR) and are lower for shorter

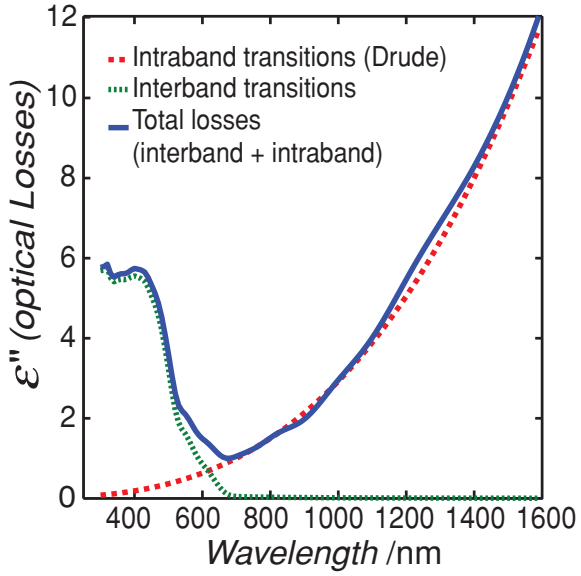

Figure 2. Imaginary permittivity or optical losses in gold:[22] the individual contributions from free electron losses (intraband transitions) and interband transition losses are shown.

wavelengths. On the other hand, interband losses in gold are high for the shorter wavelengths in the visible range. These additional losses at optical frequencies caused by interband transitions make metals such as gold and silver unsuitable for many plasmonic and metamaterial devices.[24]

Many applications, such as transformation-optics devices, require that the imaginary part of a metal's dielectric function be small. The imaginary part of permittivity depends on three important loss mechanisms: interband transitions, intraband transitions and additional scattering losses due to defects in solids.[23] Even if interband transitions are absent in the metal, intraband transitions and scattering losses are invariably present and often result in large overall losses. In order to understand the origin of this problem, a closer look at the free-electron response in a metal is helpful. The free-electron response in metals can be described by the Drude model[25,26] as shown in Equation 1.

$$\varepsilon(\omega) = \varepsilon' + i\varepsilon'' = \varepsilon_b - \frac{\omega_p^2}{(\omega^2 + \gamma^2)} + i\frac{\omega_p^2 \gamma}{(\omega^2 + \gamma^2)\,\omega} \quad (1)$$

Here ε_b is the polarization response from the core electrons (background permittivity), ω_p is the plasma frequency and γ is the Drude relaxation rate. Relaxation rate is responsible for scattering/ohmic losses and scales directly with the imaginary part of the dielectric function. Similarly, the square of the plasma frequency, ω_p^2, which is proportional to carrier concentration (n), also scales directly with ε''. Hence, a small ε'' can be achieved either by small γ or by a smaller carrier concentration, or preferably both. Attempts have been made to reduce γ in conventional plasmonic materials (noble metals) by cooling them to cryogenic temperatures.[27] However, the improvement in losses is not sufficient for practical devices. In conventional plasmonic materials the carrier concentration is very large ($\approx 10^{23}$ cm^{-3}), and this therefore significantly increases the value of ε'' in the NIR and visible regions. Decreasing the carrier concentration in these metals would be useful in significantly reducing the magnitude of ε''.

The high loss in conventional plasmonic materials is but one of the major disadvantages in using metals like gold and silver in plasmonics, optical metamaterials and TO. One issue is that the magnitude of the real part of the permittivity is very large in conventional metals.[24] This is a problem in designing many TO devices because these devices often require meta-molecules with a nearly balanced polarization response.[18,28] In other words, the polarization response from the metallic components should be of the same order as that from the dielectric components within each meta-molecule. When the real parts of permittivity of the metal and dielectric are on the same order, the geometric fill fractions of the metal and dielectric can be readily tuned to match the design requirements. On the other hand, if the magnitude of the magnitude of the real part of permittivity of the metal is a few orders larger than that of the dielectric, the metal fill fraction in the meta-molecule will be a few orders smaller than that of the dielectric. This constraint would necessitate very tiny metal inclusions in the meta-molecule, which poses a number of problems especially in terms of successful nanofabrication. Thus, having smaller magnitudes of ε' for plasmonic materials would be advantageous in many applications. The origin of the large magnitude of ε' in noble metals can be traced to their very large carrier concentrations. From Equation 1, we see that the magnitude of ε' scales almost directly with ω_p^2 or carrier concentration (n). Thus, reducing the carrier concentration in noble metals would help in reducing the magnitude of ε'.

Aside from the issues of loss and not adjustable dielectric permittivity described above, metals also pose nanofabrication challenges, especially when grown as thin films. Metal thin films exhibit quite different morphologies when compared to bulk metal, which can lead to the degradation of optical properties.[29–32] First of all, ultrathin metal films deposited by common techniques such as evaporation or sputtering often grow as semi-continuous or discontinuous films. Metal films exhibit a percolation threshold in the film thickness when grown on commonly used substrates such as glass, quartz, sapphire and silicon.[33,34] Overcoming this limit would require extra efforts such as using a wetting layer[35–38] or a lattice-matched substrate.[39,40] However, these approaches have limitations in terms of design integration and scalability. Generally, thin metal films exhibit a structure composed of many small grains. In contrast, thick films are typically composed of large grains, and their optical properties resemble those of the bulk material. When the films are thin, the grainy structure causes additional grain-boundary scattering for free electrons and increases the losses in the metal.[41,42] This description can be easily understood with the help of the permittivity function (ε) of a metal. The free electron response in metals can be described by the Drude model as shown in Equation 1. It is γ that describes the scattering/ohmic loss mechanism in the conduction electrons of metals. γ is a phenomenological parameter that is dependent on the internal grain size of the metal film. When the grain size is large, as in a bulk metal, the relaxation rate is given by γ_0. When the grain size is small, as in the case of thin metal films, Equation 2 describes the enhanced relaxation rate that arises from additional grain-boundary scattering:[43–45]

$$\gamma = \gamma_0 + A\frac{v_F}{d} \quad (2)$$

where A is a dimensionless empirical constant, v_F is the Fermi velocity of the electrons in the metal and d is the average grain size. Smaller grains result in a larger γ and, hence, higher losses. Losses in thin metal films can increase nearly three-fold due to grain-boundary scattering. In order to avoid such additional losses in conventional plasmonic materials, single-crystal growth of noble metal films has been attempted.[46,47] The improvement in losses is evident, but it is not substantial due to the limitations that arise from the nanopatterning of the metal films.

Another loss mechanism that appears in nanopatterned metal films is related to surface roughness.[48,49] Nanoscale patterning invariably results in rough surfaces and edges, which cause additional scattering and optical losses. This effect can be empirically described by an additional increment in γ. In total, the increase in γ from its bulk value is captured in a loss factor as described in Equation 3.[45] Experimental findings suggest that a loss factor of 3 to 5 is common in nanopatterned gold and silver films.

$$\gamma = (\text{Loss factor}) \times \gamma_0 \quad (3)$$

Another important issue to consider in the context of realistic devices and integration is the chemical stability of the materials. The degradation of metals on exposure to air/oxygen or humidity would pose additional problems in fabrication and integration of devices. Among conventional plasmonic materials, silver and copper are well known to degrade in air, but gold is very stable in air. While copper forms a native oxide layer in air,[50,51] silver is sensitive to sulfidation and tarnishes to form a layer of silver sulfide.[52–54] The tarnishing of these metals has a direct consequence on their optical properties, and the optical losses increase, which in turn results in larger values of the imaginary part of the dielectric function.

Another important technological challenge associated with noble metals is that they are not compatible with standard silicon manufacturing processes. This precludes plasmonic and metamaterial devices from leveraging on standard nanofabrication technologies. This also diminishes the possibility of integrating plasmonic and metamaterial components with nanoelectronic components. The compatibility issue with noble metals arises from the fact that these metals can diffuse into silicon to form deep traps, which severely affects the performance of nanoelectronics devices.[55–57] Hence the integration of noble metals into silicon manufacturing processes is a difficult challenge. Recently, copper has being incorporated into silicon processes, but additional, special processing steps are needed to create diffusion barriers between the silicon and the copper.[58,59] Gold and silver still remain outside the realm of feasibility for silicon manufacturing processes.

Major drawback of metals is that their optical properties cannot be tuned or adjusted easily. For example, the carrier concentration of metals cannot be changed much with the application of moderate electric fields, optical fields, or temperature, etc. Hence, in applications where switching or modulation of the optical properties is essential, metals are not the convenient choices.

With all the shortcomings of conventional plasmonic materials, researchers have been motivated to search for better alternatives.[24,60,61] Many alternatives to metals have been proposed that overcome one or more of the drawbacks mentioned above. The significance of a particular alternative depends on the end application, but general criteria for the choice of an alternative plasmonic material can be outlined from the issues raised in the preceding discussions.

In the following sections, we review the concept of an ideal plasmonic material and discuss its feasibility. We identify two routes to realizing a good alternative plasmonic material. The two approaches are discussed in detail and cover different material systems, including popular semiconductors, transparent conducting oxides, ceramic nitrides, silicides and other intermetallics. This overview is followed by a brief discussion on 2D materials that can support plasmons. The subsequent section discusses the merits and shortcomings of each material system for different classes of metamaterial and plasmonic applications, such as localized surface plasmon resonance (LSPR) devices, surface plasmon-polariton (SPP) waveguides, resonant metamaterials such as negative-index metamaterials, TO devices such as cloaks, hyperbolic metamaterials (HMMs), epsilon-near-zero (ENZ) devices, and finally tunable metamaterials. We conclude with a summary and outlook on the emerging research field of alternative plasmonic materials.

4. Elusive Lossless Metals

A material with a purely real and negative permittivity ($\varepsilon'' = 0$ and $\varepsilon' < 0$) would be an ideal candidate to replace metals in most of the plasmonic and metamaterial devices. Such a material produces a metallic response to light while exhibiting zero losses. However, it is impossible to have zero losses and negative permittivity simultaneously for all frequencies in any dispersive material due to the causality condition.[62] All is not lost, though–there can be a frequency interval in which the permittivity is purely real and negative. This is possible without violating causality only when there are large losses present at lower frequencies. A theoretical solution satisfying this requirement has been proposed by Khurgin and Sun.[63] **Figure 3** shows two possible electronic band structures for a metal.

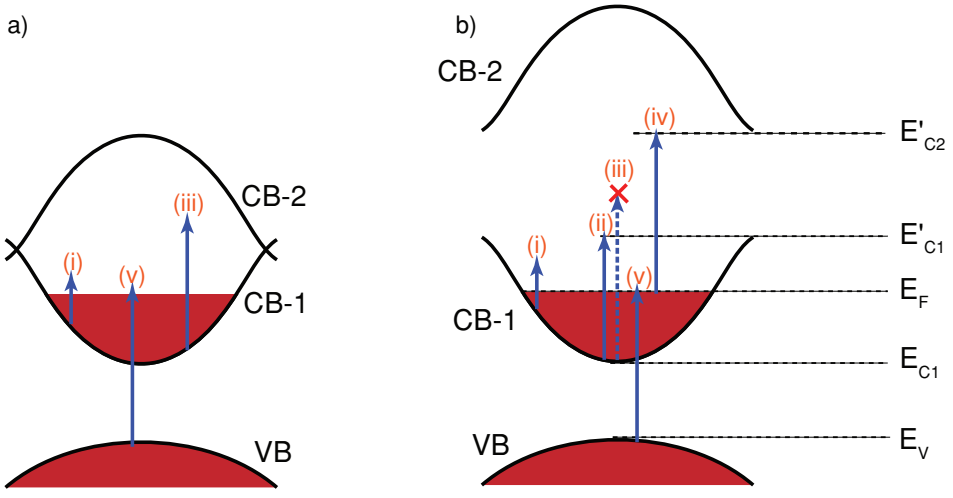

Figure 3. A schematic showing bandstructures of a) metal with losses b) metal with no losses in a specific wavelength range. The arrows (labeled (i) through (v)) show the electronic transitions upon absorption of a photon of the corresponding energy. Redrawn from ref.[63]

Figure 3a resembles the band structure of many common metals. Suppose, however, that a metal possesses an electronic band structure as shown in Figure 3b. In this case, there could be a frequency range where optical losses due to electronic transitions (photo-generation of electron-hole pairs) can go to zero. Figure 3 shows three energy bands of the metal: a completely filled valence band (VB), an incompletely filled conduction band (CB-1) and a completely empty conduction band (CB-2). The energies of the ends of the bands are as indicated in the figure. When a photon of energy E less than $(E'_{C1} - E_{C1})$ impinges on this material, an electron in CB-1 can absorb the photon and make an intraband transition. This is indicated by the label (i) in Figure 3. Intraband transitions lead to large optical loss at low frequencies, similar to the losses observed in any Drude metal. Intraband transitions occur until the photon energy increases to $(E'_{C1} - E_{C1})$ (label (ii) in the figure). When the energy of photon E is slightly greater than $(E'_{C1} - E_{C1})$, there are no allowed states for any electronic transition in the case of Figure 3b. Thus, a metal depicted by Figure 3b is lossless at this photon energy. Notice that this situation never occurs in the case of Figure 3a. The lossless regime lasts as long as the photon energy is less than the lower of $(E'_{C2} - E_F)$ and $(E_F - E_V)$ because there are no allowed electronic transitions due to the unavailability of energy states. In other words, the joint density-of-states (JDOS) for the photon energy E is zero. Hence, the optical loss falls to zero ($\varepsilon'' = 0$) in the range of energies from $(E'_{C1} - E_{C1})$ to the smaller of $(E'_{C2} - E_F)$ and $(E_F - E_V)$. For photon energy greater than $(E'_{C2} - E_F)$, interband transitions from CB-1 to CB-2 introduce optical losses (label (iv) in the figure). For a photon energy greater than $(E_F - E_V)$, interband transitions from VB to CB-1 contribute to optical losses (label (v) in the figure). The intraband transitions occurring at low photon energies present a polarization response that is adequate to produce a negative real permittivity, while the special band structure can produce zero losses in a band of photon energies. Thus, it is theoretically possible to have a metal that is lossless in a desired frequency range.

The fact that none of the known metals have this specific band structure explains why natural metals are always with associated losses. In other words, there are no naturally occurring materials that are simultaneously lossless and have negative real permittivity in any part of spectrum. Khurgin and Sun[63] suggested that stretching the sodium metal lattice by nearly a factor of two would make sodium satisfy the conditions for being metallic ($\varepsilon' < 0$) and loss-free in the mid-IR. The paper also provides tight-binding calculations of the band structure and, thereby, the dielectric function of lattice-stretched sodium and shows that such a material is metallic and lossless for wavelengths from 1.8 μm to 2.4 μm. Though this result is conceptually important, its practicality is not evident. Khurgin and Sun[63] also suggest techniques that could possibly stretch the lattice spacing between metal atoms. One of their proposed techniques is to incorporate foreign atoms in the metal lattice to stretch the lattice. As an example, AlO is metallic with the inter-Al spacing increased by the addition of oxygen atoms. Such possibilities require careful consideration of how the band structure would be modified by the foreign atoms and how the contribution to the free-electron cloud would be affected. In the case of AlO, every oxygen nucleus bonds to two aluminum electrons, thereby reducing the concentration of free electrons in aluminum. This changes not only the electronic band structure, but also the conduction-band electron distribution. Considering the fact that there are no lossless metals found so far in nature, lossless metals remain an elusive goal.

Although naturally occurring loss-free metals may not exist, incorporating gain into the structure of a metal in order to compensate for losses is an engineering strategy that has worked well.[64–69] Gain media such as organic dyes, quantum dots, and solid-state materials including semiconductor structures can provide the amplification necessary to partially or fully compensate losses. Most of these techniques are resonant mechanisms and, hence, are narrowband. Also, the practical losses in noble metals are so high that enormously large gain is essential to compensate the losses. Additionally, incorporating gain complicates fabrication and adds noise to the device. Thus, it would be more practical to have a metal with much smaller losses than those in noble metals even though the material may not be completely loss-free. Supposing that losses would be tolerable if they can be scaled down from the high-loss levels of noble metals, many solutions become possible for each wavelength range. Carefully observing the dielectric function described by the Drude model (Equation 1), we notice that reducing γ can directly scale down the losses. Many possibilities have been explored in reducing the carrier-damping losses in metals.[27,70–72] However, the losses could not be reduced significantly in the optical range.

Another possibility for reducing loss in metals is to reduce ω_p, which can reduce the magnitudes of both of the real permittivity and the imaginary permittivity. However, ω_p should not be reduced too much to retain a metallic response in the desired wavelength range. This lower limit on ω_p can be deduced from the Drude-model description of $\varepsilon'(\omega)$. If we require metallic behavior ($\varepsilon'(\omega) < 0$) for frequencies less than the cross-over frequency ($\omega < \omega_C$), then $\omega_p > \sqrt{\varepsilon_b(\omega_C^2 + \gamma^2)}$. This also sets the lower limit on the imaginary part of permittivity: $\varepsilon''(\omega) > \frac{\varepsilon_b \gamma}{\omega_C}$ for $\omega < \omega_C$. Both of these limits are useful in assessing and engineering different materials and their optical properties to produce alternative plasmonic materials.

There are two possibilities in producing alternative plasmonic materials based on the Drude description. One of them is to dope semiconductors heavily and create enough free carriers that the material's optical properties become metallic in the desired wavelength range.[73,74] The other option is to remove excess free carriers from metals so as to reduce the carrier concentration to the desired value.[75,76] Both of these techniques have their own benefits from the perspective of material design. The details of the two approaches and the recent developments based on them are discussed in the following sections.

Plasmonic materials are not necessarily Drude metals. The concept of a lossless metal discussed above is an example that does not follow the Drude model of free carriers. Metallic properties can be produced by a strong resonance as well. This concept can be appreciated better by considering a two-level atomic system. The optical response of a two-level system is described by the Lorentz model:

$$\varepsilon(\omega) = \varepsilon_b + \frac{\omega_{p,12}^2}{\omega_{12}^2 - \omega^2 - 2i\omega\gamma_{12}} \quad (4)$$

where ε_b is the background permittivity, ω_{12} is the energy difference between levels 2 and 1, γ_{12} is the damping co-efficient of the resonance, and $\omega_{p,12}$ is the strength of the resonance. $\omega^2_{p,12}$ is proportional to the density of oscillators per unit volume. When $\omega > \omega_{12}$, the real permittivity can be less than zero depending on the strength of resonance. The losses associated with the resonance depend on γ_{12}. Thus, a metallic response can be produced by the resonant absorption of photons in this material. Such materials are found abundantly in nature with varying properties and strengths of their resonances. For example, many organic molecules such as dyes absorb in specific wavelength bands due to electronic transitions. When many such molecules are packed closely together as in a thin film, strong resonances can be achieved. This can produce a metal-like response for light.[77,78] The only drawbacks of this approach are that this phenomenon is associated with losses, and it is narrowband.

There are a few other techniques that can produce low-loss metals. One of these techniques is to use or design a material with nearly zero loss resulting from electromagnetically induced transparency (EIT).[79] The nonlinear optical phenomenon responsible for EIT can render a material lossless to resonant laser radiation. In a material with two resonant absorption frequencies, the material can become nearly lossless at one of the resonances if a strong saturating field acts at the other resonance frequency.[80–82] In this scenario, the real permittivity of the material may switch from negative to positive around the resonance frequency where the losses are nearly zero. Thus, there can be a band of frequencies close to the resonance for which the real permittivity is negative and the losses are nearly zero. This phenomenon depends on the resonant nonlinear interaction of optical fields and, hence, is narrowband. Also, the phenomenon requires materials that possess a particular electronic structure. An additional disadvantage of this phenomenon is that it can require high-intensity optical excitation to produce a significant nonlinearity. Despite these disadvantages, however, the EIT mechanism can in principle produce nearly lossless metals.

As described above, there are many techniques in which losses in metals could be reduced. However, the technologically important techniques are those which could be easily realizable and integrated into devices. Tailoring Drude metals by altering their plasma frequencies is a technique that does not pose any major technological limitation and hence, is a very useful approach. Previously, two popular strategies were mentioned that can tailor-make metals: turning a semiconductor into a metal by heavy doping, and reducing the carrier concentration in a metal to cause it to become less metallic. We will review these two techniques and their applications in detail in the following sections.

5. Semiconductors to Metals

Increasing the carrier concentration in semiconductors enough to cause them to behave like metals is accomplished through doping. Achieving metal-like optical properties ($\varepsilon' < 0$) in the spectrum of interest puts a lower limit on the carrier concentration that must be achieved by doping. The optical response of free carriers as described by the Drude model (Equation 1) can be used to estimate this minimum carrier concentration. To obtain metal-like properties ($\varepsilon' < 0$) for $\omega < \omega_C$, the lower limit on the plasma frequency (ω_p) and hence the carrier concentration (n) is given by Equation 5:

$$\omega_p^2 > \varepsilon_b(\omega_C^2 + \gamma^2)$$
$$n > \frac{\varepsilon_0 m^*}{e^2}\varepsilon_b(\omega_C^2 + \gamma^2) \quad (5)$$

where ε_0 is the vacuum permittivity, e is the electron charge, and m^* is the effective mass of the carrier. **Table 1** shows the estimates of carrier concentration that would be required for many common semiconductors in order to obtain $\varepsilon' = -1$ at the technologically important telecommunication wavelength

Table 1. Comparison of different heavily-doped semiconductors as potential alternative plasmonic materials. The table evaluates the carrier concentration required to reduce the real permittivity of semiconductors to $\varepsilon' = -1$ at telecommunication wavelength ($\lambda = 1.55$ μm). The electronic parameters of the semiconductors reported in the literature are used in Drude model to evaluate the optical properties in the NIR.

Material	Background permittivity (ε_b)	Carrier mobility when heavily doped[a] [cm^2 V^{-1} s^{-1}]	Effective mass (m^*)	Relaxation rate [eV]	Carrier concentration required to achieve Re{ε} = −1 at $\lambda = 1.55$ μm [× 10^{20} cm^{-3}]	Im{ε} or losses at $\lambda = 1.55$ μm
n-Si[318,319]	11.70	80[320]	0.270	0.0536	16.0	0.8508
p-Si[319]	11.70	60[320]	0.390	0.0495	23.1	0.7853
n-SiGe[321]	15.10	50[322]	0.24	0.0965	18.2	1.9414
n-GaAs[124]	10.91	1000[323][b]	0.068	0.017	3.76	0.2534
p-GaAs[127]	10.91	60	0.44[324]	0.0438	24.4	0.6528
n-InP[123,325]	9.55	700	0.078	0.0212	3.82	0.2796
n-GaN[136–138]	5.04	50	0.24	0.0965	6.83	0.7283
p-GaN[136–138]	5.24	5	1.4	0.1654	42.3	1.290
Al:ZnO[326]	3.80	47.6	0.38	0.064	8.52	0.384
Ga:ZnO[327]	3.80	30.96	0.38	0.0984	8.59	0.5904
ITO[328]	3.80	36	0.38	0.0846	8.56	0.5077

[a]Mobility values used in the calculations; [b]Mobility corresponding to the free electron concentration of 1×10^{19} cm^{-3}.

(λ = 1.55 μm). In this scenario, ω_C (cross-over frequency) is slightly higher than the telecommunication frequency. For many of the common semiconductors such as silicon, the minimum carrier concentration to obtain metal-like optical properties in the NIR is about 10^{21} cm^{-3}. Smaller ε_b and m^* values would slightly reduce the minimum carrier concentration, but a high carrier density is inevitable for achieving metal-like properties in the NIR. Such high carrier densities require ultrahigh doping densities, which poses major limitations. The challenges in ultrahigh doping will be discussed in the latter part of this section.

Another issue to be considered when choosing a semiconductor for creating metal-like behavior is the mobility of the carriers. The Drude relaxation rate (γ) can be related to the mobility (μ) of the charge carrier at a given optical frequency by Equation 6:

$$\gamma = e/\mu m^* \quad (6)$$

Reducing the damping loss requires that the product of mobility and effective mass must be as large as possible. Mobility degrades significantly with higher doping levels due to increased impurity scattering.[83] Hence, it is important to consider appropriate mobility numbers when assessing various semiconductors. Table 1 shows the approximate values of γ evaluated using Equation 6 where low-frequency m^* and high-doping mobility ($\geq 10^{19}$ cm^{-3}) values are used. The damping losses in semiconductors are comparable to those of bulk gold (0.07 eV) and silver (0.02 eV) as reported by Johnson and Christy.[22]

Another consideration in choosing semiconductors is their optical bandgap. The optical bandgap corresponds to the onset of interband transitions, which cause additional optical losses. Hence, the optical bandgap needs to be larger than the frequency spectrum of interest. Table 1 lists common semiconductors whose optical bandgaps correspond to the NIR or higher photon energies. Clearly there are many semiconductors that can be useful for applications in the NIR and longer wavelengths only if they can be doped heavily. From Table 1, we note that the only major bottleneck in turning semiconductors into low-loss plasmonic elements at optical frequencies is accomplishing the required ultrahigh doping. A deeper understanding of the doping mechanism in semiconductors can provide insights for accomplishing this ultrahigh doping, and hence we turn our attention to this process next.

Doping is a process of incorporating foreign atoms or impurities into the lattice of a semiconductor to controllably change the properties of the semiconductor. When certain atomic species are incorporated into the lattice sites of the semiconductor, the free-carrier concentration in the material can be changed proportionally. For our purposes, we will only consider doping that acts to increase the free-carrier concentration. When dopant atoms replace (substitute) the semiconductor atoms in the lattice, this form of doping is called substitutional doping, which effectively contributes to an increase in the charge-carrier density in the material. When the dopant atom occupies an interstitial site, it is called interstitial doping. Interstitial doping is an ineffective doping method because it does not contribute any free carriers and, therefore, does not producing any electrical doping.[84] There is another mechanism called doping compensation that can also result in ineffective doping. In this mechanism, dopants such as silicon in GaAs can behave as both an p-type and n-type dopant and self-compensate any net doping effect.[85,86] Doping is also limited on the higher side by the solid solubility of the dopant in the semiconductor.[87,89] Introducing dopants more than the solid-solubility limit may result in phase separation of dopants or compounds of dopants. This phase separation of excess dopants leads to ineffective doping. Often, ultrahigh doping results in more crystal defects, which could act as traps for free carriers. These trap states can counter the effect of doping and thus reduce the carrier concentration. In general, the doping mechanism is complicated and, most often, not all dopant atoms succeed in contributing free charge carriers due to a number of reasons, including those mentioned above.[84] Thus, doping efficiency is an important quantity and can be defined as the fraction of dopants that contribute to the charge carrier density. Doping efficiency decreases sharply for high doping concentrations in many semiconductors, making ultrahigh doping a tough challenge. Although there are many different material engineering approaches that can provide elegant solution to this problem, a straightforward approach to the problem of achieving ultrahigh doping would be to choose a dopant that has very high solid-solubility limit in the selected semiconductor material. This approach has been utilized in demonstrating many semiconductor-based plasmonic materials. A few recent reports on the demonstration of plasmonic properties of heavily-doped semiconductors are reviewed in the following sections.

5.1. Silicon

Silicon is the semiconductor platform that has paved our way into the information age. Nanofabrication technologies have rapidly advanced to such an extent that mass production has become possible, which has made silicon technology ubiquitous. Ultrahigh integration capabilities and precise control of the materials and geometry at the nanoscale are advantages of silicon technology, and these advantages can be leveraged for new devices and systems. For this reason, many other technologies such as micro-electromechanical systems (MEMS) and photonics are being developed based on silicon platform and silicon materials engineering. Silicon photonics has already made its way to commercialization.[90] Shifting from photonics to plasmonics could provide significant benefits in terms of integration density. Silicon plasmonics[91–93] could be easily possible if heavily doped silicon can be used as a metallic component. Turning silicon metallic at the telecommunication wavelength requires very high doping and is very challenging for the reasons discussed below. However, silicon can be turned metallic at longer wavelengths. To motivate our discussion, we next focus on the recent developments in silicon plasmonics, the limitations of the technology, and the challenges in achieving plasmonic silicon.

Silicon can be doped n-type by Group V elements such as phosphorous, arsenic and antimony, and it can be doped p-type by Group III elements such as boron, aluminum and gallium. Conduction electrons in silicon have much smaller effective mass compared to holes in silicon[94] and hence, the plasma frequency will be higher for n-type silicon compared to p-type for

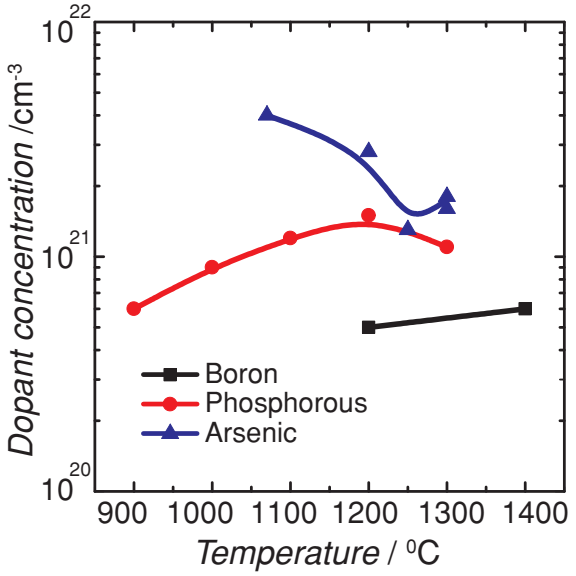

Figure 4. Solid solubility curves for three different dopants in silicon as a function of doping temperature (replotted from data in ref.[87]).

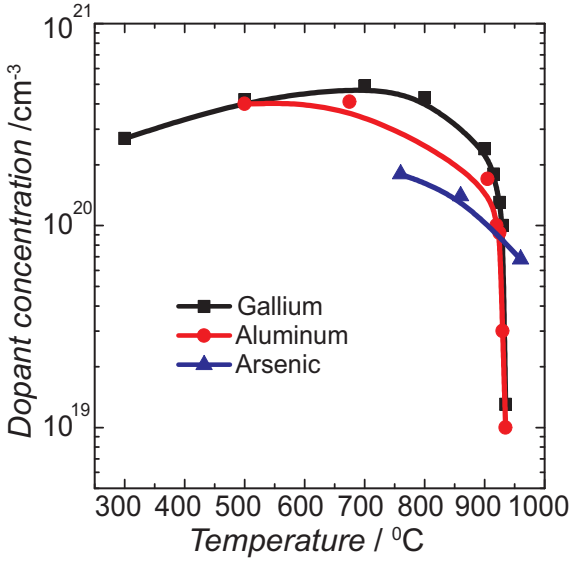

Figure 5. Solid solubility curves for three different dopants in germanium as function of processing temperature. Replotted from data in ref.[87]

the same doping level (see Equation 5). In spite of the low effective mass of conduction electrons in silicon, the n-type doping required for turning silicon metallic at the telecommunication frequency is still very high (see Table 1). Thus, it is essential to study the solid-solubility limits and doping efficiency for various dopants.

The solid-solubility curves for some of the more soluble dopants in silicon[87] are shown in **Figure 4**. Phosphorous has the highest solid solubility at about 10^{21} cm^{-3}, followed by arsenic and boron. Although the solid solubility is high, the doping efficiency decreases when the doping concentration approaches the solubility limit.[95,96] Increasing defect densities and alloying effects start to dominate at such high doping levels, making ultrahigh doping of silicon a challenge. Recently, there have been many studies on the plasmonic properties of heavily-doped silicon.[97,98] The plasmonic property of diffusion-doped silicon has been confirmed in the infrared range (in the wavelength of 8–10 μm) for boron doping densities of about 10^{21} cm^{-3}.[99] Ion-implantation has been reported to lower the doping efficiency significantly compared to diffusion doping.[100] Even with diffusion doping, the doping efficiencies are not high enough to achieve carrier concentrations of 10^{21} cm^{-3}. Thus, pushing the plasma frequency further into the NIR and achieving plasmonic properties at the telecommunication frequency in silicon remains an open challenge.

5.2. Germanium

Germanium is another standard semiconductor that is commonly used along with the silicon platform for electronic devices. Germanium is attractive for its higher electron mobility[101] and smaller optical bandgap than silicon, which can allow the fabrication of photodetectors at the telecommunication frequency.[102–105] Furthermore, by incorporating silicon into germanium with varying concentrations, the material properties can be tuned.[106–108] However, a major problem with Ge as a plasmonic material at the telecommunication frequency is its absorption due to interband transitions. At lower frequencies, germanium is transparent and may be highly doped to produce plasmonic properties. Compared with Si, the ε_b value is higher for Ge, which necessitates higher doping to achieve metallic properties at a given wavelength. Similar to silicon, the solid-solubility limits for dopants in Ge do not permit such high doping. **Figure 5** shows the solid solubility curves for highly soluble dopants in Ge.[87] Gallium has the highest solubility in germanium, followed by aluminum and arsenic. However, the numbers are nearly an order of magnitude smaller than those of silicon. Hence, it is even more challenging to heavily dope germanium to turn it plasmonic in the optical range. Nevertheless, many alloys of Si and Ge such as $Si_{1-x-y}Ge_xSn_y$ are being investigated for the possibility of plasmonic behavior at the telecommunication wavelength.[109]

5.3. III–V Semiconductors

In recent decades, III–V semiconductors have provided the materials platform for many technologies such as high-speed switching,[110,111] power electronics,[112,113] and optoelectronics.[114–117] These materials exhibit a wide tunability in the optical bandgap that can be controlled by varying the composition of their ternary and quaternary compounds.[118–120] Since integrating plasmonics and metamaterial devices on optoelectronics platforms would be a very important development, studying the possibility of plasmonic properties with these materials is a very relevant step toward this goal. In the following sections we discuss the possibilities for plasmonic properties from III–V semiconductor systems.

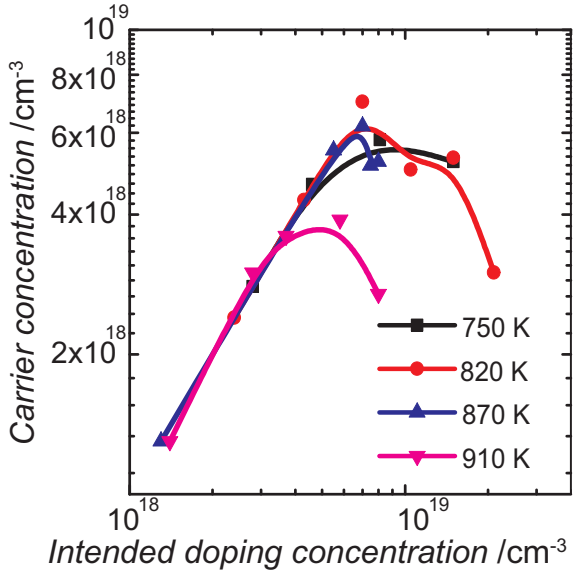

Figure 6. Doping efficiency for silicon in epitaxial GaAs grown by molecular beam epitaxy at different substrate temperatures. As_4 source was used for this data set. Replotted from data in ref.[126]

5.3.1. Arsenides and Phosphides

Compounds of III–V semiconductors, such as those based on GaAs and InP, are semiconductors with an optical bandgap in the NIR. This is useful to know because a bandgap comparable to that of silicon results in a value of ε_b that is comparable to that of silicon for these materials.[121,122] In addition, the electron mobility is very high in these materials due to a small effective mass.[123,124] This relaxes the carrier concentration requirement for observing metallic properties in the NIR (see Table 1). In these materials, a carrier concentration in excess of 10^{20} cm^{-3} is required to observe plasmonic properties at the telecommunication wavelength. However, such high doping is very challenging in these materials owing to lower solid solubilities of the dopants and poor doping efficiency.[125] Doping higher than 10^{19} cm^{-3} is known to produce effects such as doping compensation. For instance, silicon is a common n-type dopant in GaAs, but at high doping levels, silicon can behave not only as an n-type substitutional dopant, but also as a p-type dopant. Thus, silicon can compensate itself at high doping densities, resulting in low doping efficiency.[85,125] **Figure 6** shows the n-type doping achieved in GaAs films grown by molecular beam epitaxy (MBE) at different growth temperatures, as reported by Neave et al.[126] N-type doping beyond 10^{19} cm^{-3} is clearly difficult in GaAs films. Many other studies report similar trends[125], and it was pointed out that the carrier concentration in GaAs shows a saturating trend for donor densities higher than 5×10^{18} cm^{-3}. On the other hand, p-doping with Be or C can be used to achieve carrier concentrations in excess of 10^{20} cm^{-3}.[127] However, holes have a higher effective mass and poor carrier mobility, which raises the minimum bar on carrier concentration to turn p-GaAs plasmonic at the telecommunication frequency (see Table 1).

Turning our attention to InAs, we see that this material can be doped higher than n-GaAs and, recently Law et al.[128] reported a carrier concentration in InAs of about 7.5×10^{19} cm^{-3}, which showed metal-like behavior for wavelengths longer than 6 μm. Law et al. demonstrated LSPR behavior in an array of cylinders of heavily doped InAs at a wavelength of 9 μm. Increasing the carrier concentration further in these semiconductors is difficult, and as a result the plasmonic applications for these materials are limited to the mid-infrared (MIR) range. Several metamaterial and plasmonic devices have been demonstrated using these materials in the MIR. Hoffman et al.[73] showed negative refraction in a so-called hyperbolic metamaterial consisting of planar, alternating layers (a superlattice) of heavily doped ($1–4 \times 10^{18}$ cm^{-3}) $In_{0.53}Ga_{0.47}As$ and undoped $Al_{0.48}In_{0.52}As$ deposited by MBE. The individual layers were 80 nm thick, and the operating wavelength was around 8 μm. Such a structure shows uniaxial anisotropy in the effective-medium limit with different signs of real permittivities in different directions. This extreme anisotropy allows negative refraction of incident TM-polarized light. This metamaterial device was shown to have a performance figure-of-merit[73] of about 20, the highest reported so far. Yet another demonstration is the epsilon-near-zero (ENZ) properties of the InAsSb material when doped heavily. Adams et al.[129] show that heavy doping ($1–2 \times 10^{19}$ cm^{-3}) of InAsSb causes the real permittivity to cross zero and turn metal-like in the MIR range. At the zero cross-over of real permittivity (occurring at about 8 μm wavelength), the material behaves as an ENZ material and exhibits special properties. In their paper, Adams et al. created a subwavelength slit underneath the ENZ layer, which causes photons from the slit to funnel through the material and experience enhanced transmission. This phenomenon was observed by Adams et al. in a InAsSb-based device.

Other than metamaterial devices, these semiconductors have been used for electric field-effect tuning of the characteristics of photonic devices. Many such demonstrations have been reported for THz and MIR devices. Kleine-Ostmann et al.[130] showed the modulation of a THz signal by field-control of carrier concentration in a GaAs/AlGaAs heterostructure. Chen et al.[131] demonstrated modulation up to 50% for a THz signal through a split-ring resonator-based metamaterial by electrically controlling the depletion width in a Au/n-GaAs Schottky junction. Jun et al.[132] extended this concept to a MIR metamaterial formed by an array of gold split-ring resonators. Shaner et al.[133] showed electrically tunable extraordinary transmission through sub-wavelength holes in a gold film operating at 8 μm wavelength. The tunability was achieved by electrically modulating the carrier concentration in a buried GaAs layer. However, none of these studies mentioned a demonstration of electrically tunable devices used semiconductors as plasmonic components. The tunability could be much higher if the semiconductors are heavily doped and used as plasmonic components.

In general, then, we find that III–V compounds excluding the nitrides have been widely studied for plasmonic applications. Their optical properties can be designed to be plasmonic in the MIR and longer wavelengths. They are useful not only as plasmonic materials, but also as electrically tunable components in this wavelength range.

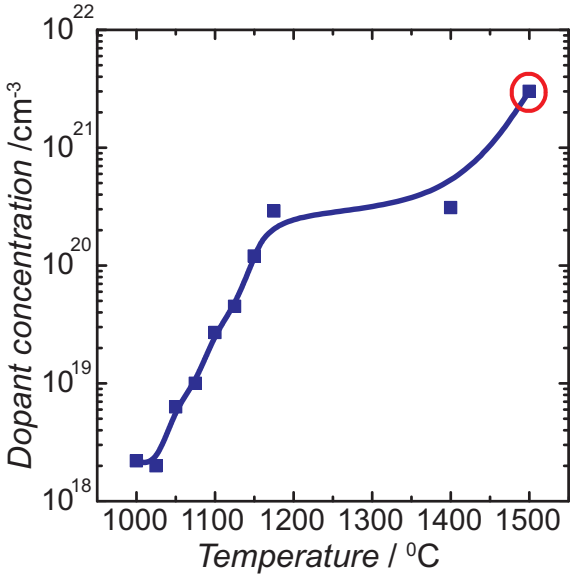

Figure 7. Electron concentration as determined by Hall measurements in the GaN layers as a function of the Ge furnace temperature. The growth temperature was maintained at 1028 °C. Replotted from data in ref.[139]

5.3.2. III-Nitrides

The semiconductor GaN is an emerging platform for optoelectronics with a capability of operation that spans all of the visible range.[134,135] Large tunability of the bandgap in InGaN ternary systems has attracted many researchers to study this material system for visible optoelectronics applications. GaN is wide bandgap semiconductor with a direct bandgap of about 3.3 eV. The wide bandgap lowers the ε_b to moderate values and, hence, reduces the minimum carrier concentration required to achieve metallic properties at a given wavelength (see Table 1). The carrier effective masses are not as small as those of GaAs or InP.[136] Hence, the Drude losses in GaN are slightly higher than that those in GaAs, but GaN can be doped n-type to a much higher level than GaAs.[137] In addition, the dopant compensation effects observed in GaAs and InP are not as restrictive in GaN.[138] Hageman et al.[139] demonstrated ultrahigh n-type doping of about 3×10^{21} cm^{-3} with Ge in GaN. **Figure 7** shows the solid solubility curves for Ge in GaN adopted from that reference.[139] The report also points out that 3×10^{21} cm^{-3} doping (marked by the red circle in Figure 7) resulted in an excessive incorporation of Ge beyond the solid-solubility limit, which altered the growth morphology significantly. Such high doping may not be necessary for plasmonic applications of GaN at the telecommunication wavelength. **Figure 8** shows the optical properties of GaN as expected from the Drude model for the data presented in ref.[136] With slightly higher doping, GaN could be turned plasmonic at the telecommunication wavelength. Clearly, GaN holds some promise for being a low-loss alternative plasmonic material in the NIR.

5.4. Transparent Conducting Oxides (TCOs)

Oxide semiconductors such as zinc oxide, cadmium oxide and indium oxide can be highly doped to make them conducting films.[140,141] Since these semiconductors have a large bandgap, they are transparent in the visible range. Hence, these materials are known as transparent conducting oxides (TCOs). Such TCOs are popular for applications in display panels where they form the electrical contacts to the pixel circuitry. One of the most popular TCOs is indium tin oxide (ITO). Because they can be doped very heavily, TCOs exhibit high DC conductivity. It is exactly this property that gives them metal-like optical properties in the NIR range. Like any other semiconductor, the optical properties of TCOs can be tuned by changing the carrier concentration/doping. They can be grown into thin films and many different nanostructures, polycrystalline and crystalline structures, patterned by standard fabrication procedures and integrated with many other standard technologies. Thus, TCOs form an obvious choice as alternative plasmonic materials in the NIR.[74] Among the many TCOs, our previous studies have

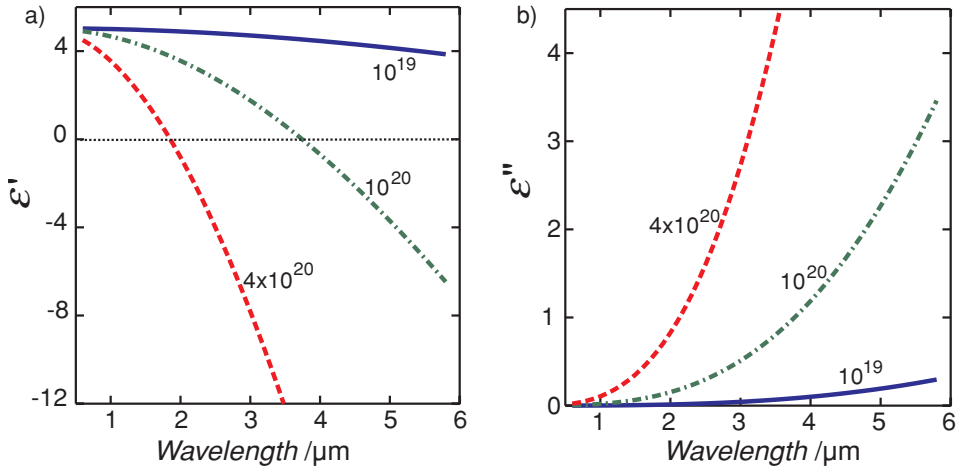

Figure 8. Optical properties of heavily doped GaN as expected from Drude model. The parameters for this calculation are taken from ref.[139] The plot shows the a) real and the b) imaginary parts of the dielectric function for doping concentrations mentioned in the units of cm^{-3}.

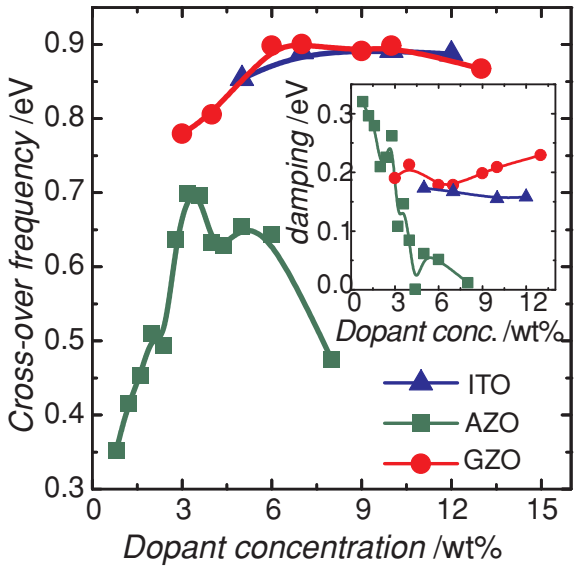

Figure 9. Cross-over frequency (frequency at which Re(ε) = 0 or screened plasma frequency) as function of dopant concentration in three TCOs: indium-tin-oxide (ITO), Ga:ZnO (GZO) and Al:ZnO (AZO).[76] The inset shows the Drude damping rate as a function of dopant concentration. All the films were deposited using pulsed laser deposition and the optical parameters are extracted using a spectroscopic ellipsometer.

shown that heavily-doped ZnO and ITO are good candidates for NIR applications.[24] In this review we focus on these specific materials in the subsequent discussions.

Thin films of TCO materials may be grown by many different techniques such as sputtering, laser ablation, evaporation, solution processing and chemical vapor deposition.[141,142] Since TCOs are non-stoichiometric oxides, their properties depend on the deposition technique used. Deposition schemes such as laser ablation and sputtering are more suitable in cases where the stoichiometry needs to be controlled to produce desired film properties. In our work, we deposit aluminum-doped ZnO (AZO), gallium-doped ZnO (GZO) and ITO thin films using the pulsed laser deposition (PLD) technique. The films are deposited by laser ablation of multiple targets using a ns-pulsed KrF (248 nm) excimer laser. The laser is focused to provide a fluence of about 2 J cm^{-2} per pulse. Multiple targets are ablated in a specific manner to achieve the desired composition of the resultant film. For example, an AZO film with specific a aluminum concentration is accomplished by repeating ablation cycles consisting of sequential deposition of alumina and zinc oxide targets with a specific number of pulses per target. By increasing the number of pulses on the alumina target while holding the number of pulses on the zinc oxide target constant, the concentration of aluminum in the resultant AZO film can be varied. The growth of separate, multilayer films is avoided by keeping the number of ablation pulses on each target small. This experimental set-up enabled us to study the maximum doping levels in these TCO films. **Figure 9** shows the carrier concentration in these TCO films as a function of doping concentration. The carrier concentration was extracted by fitting the Drude model to the measured data. Optical characterization was carried out using a spectroscopic ellispometer (J.A. Woollam Co.). The films were deposited under an oxygen partial pressure of 1 mTorr. Our results indicate that AZO shows lower losses with higher doping because of improved crystallinity in the highly doped films. However, the highest carrier concentration achieved is smaller in AZO than in ITO or GZO. The losses are higher with GZO and ITO, but much higher carrier concentrations are possible in these films. When the oxygen partial pressure was decreased below 1 mTorr, the resultant AZO films exhibited higher carrier concentrations and performed the best compared to the other two materials. **Figure 10** shows the optical properties of TCO films extracted from ellipsometry measurements. The retrieval of the dielectric functions of TCOs was based on Drude-Lorentz model. Drude model was added to account for the free carriers and the Lorentz oscillator was added in UV to account for the interband transitions at the band edge. **Table 2** shows the parameters of Drude-Lorentz model for AZO, GZO and ITO retrieved from

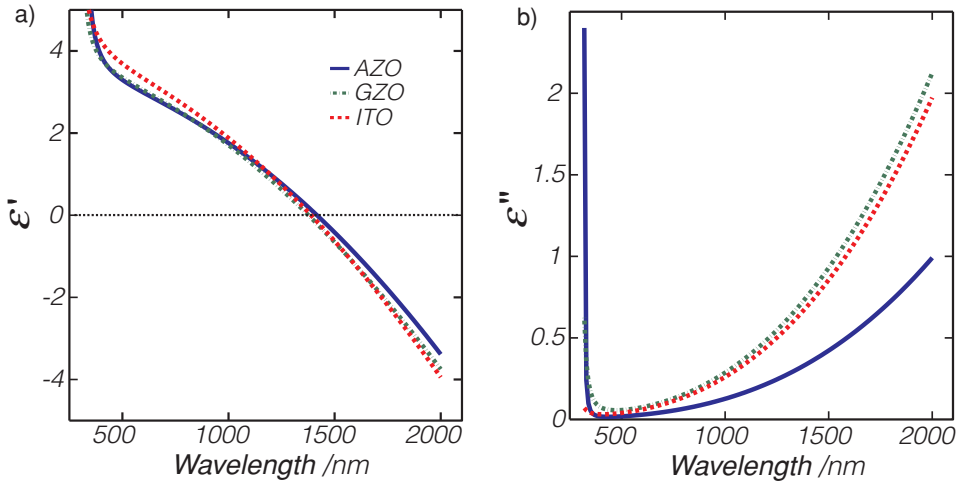

Figure 10. a) Real and b) imaginary parts of dielectric function of TCO films: Al:ZnO (2 wt%), Ga:ZnO (4 wt%) and ITO (10 wt%) deposited using pulsed laser deposition. The deposition conditions were optimized to produce lowest losses and highest plasma frequency.

Table 2. Drude-Lorentz parameters of five alternative plasmonic materials retrieved from ellipsometry measurements. The dielectric function of the materials may be approximated in the wavelength range of 350–2000 nm by the equation: $\varepsilon(\omega) = \varepsilon_b - \frac{\omega_p^2}{\omega(\omega + i\gamma_p)} + \frac{f_1\omega_1^2}{(\omega_1^2 - \omega^2 - i\omega\gamma_1)}$, where the values of the parameters are as listed in the table.

	AZO (2 wt%)	GZO (4 wt%)	ITO (10 wt%)	TiN (deposited at 800 °C)	TiN (deposited at 500 °C)	ZrN
ε_b	3.5402	3.2257	3.528	4.855	2.485	3.4656
ω_p [eV]	1.7473	1.9895	1.78	7.9308	5.953	8.018
γ_p [eV]	0.04486	0.1229	0.155	0.1795	0.5142	0.5192
f_1	0.5095	0.3859	0.3884	3.2907	2.0376	2.4509
ω_1 [eV]	4.2942	4.050	4.210	4.2196	3.9545	5.48
γ_1 [eV]	0.1017	0.0924	0.0919	2.0341	2.4852	1.7369

ellipsometry measurements. Clearly, AZO is the TCO with the lowest loss, followed by ITO and then GZO. However, optimizing the films for maximum carrier concentration in AZO is more difficult compared to the other two TCOs.

In our studies, we also found that TCO films show thickness-dependent optical properties.[76] This is mainly attributed to the interfacial defects at the TCO/substrate interface.[143,144] These defects trap carriers and reduce the carrier concentration of the films. Overall, films thicker than about 50 nm were showed little dependence of their optical properties on the thickness.[76]

Patterning of TCO films is an important step towards TCO-based plasmonic devices. TCO films can be patterned on the micro- and nanoscale using standard fabrication techniques. In particular, nanostructures in TCOs may be created using electron-beam lithography followed by reactive-ion etching (RIE), wet chemical etching or lift-off.[142] **Figure 11** shows the scanning electron microscope (SEM) image of an array of nanodisks formed by a lift-off process in a GZO film.[145] In this case, an electron-beam resist (ZEP-520A) was patterned on a glass substrate, and a GZO film was deposited on top of this structure. Then a lift-off process was used to obtain GZO disks arrays. The lift-off process limits the minimum feature size that can be patterned because the resist hardens during the deposition of the GZO film and poses difficulties in removing small features. This problem can be overcome by using an etching technique instead. Notably, an RIE procedure with chlorine chemistry works well for GZO and AZO films, while ITO can be patterned by fluorine chemistry. The SEM images of gratings formed from an AZO film using RIE are shown in **Figure 12**.[145] Compared with the lift-off structures as shown in Figure 11, we see that the RIE process produces more vertical sidewalls. Wet chemical etching can also be performed on any of the three TCOs with a 1:50 diluted HCl or 1:20 diluted tetramethyl ammonium hydroxide (TMAH) solution. AZO and GZO etch faster in both acidic and alkaline solutions, while ITO etches slowly. In conclusion, this initial demonstration of nanostructures using TCOs is a first step, and clearly these techniques may be extended to fabricate other, more complicated geometries.

Transparent conducting oxides can be deposited on many different substrates, including flexible polymer substrates.[146,147] In addition, they can be used to produce 3D structures or can be deposited conformally on 3D patterned polymers. Frolich and Wegener[148] showed that heavily doped ZnO can be deposited

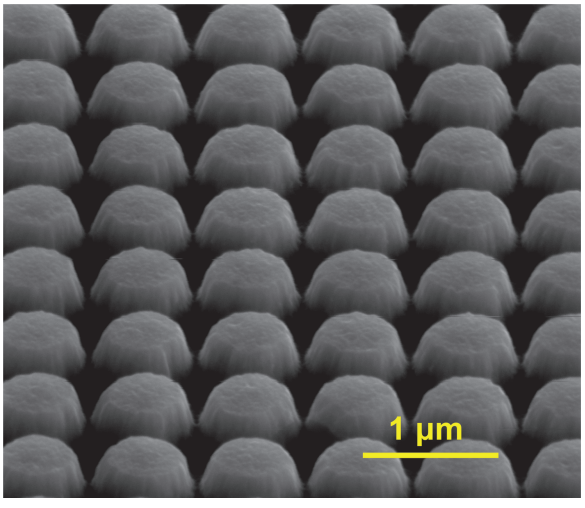

Figure 11. Scanning electron micrograph image of GZO nanodisks fabricated by e-beam lithography and lift-off processes.[145]

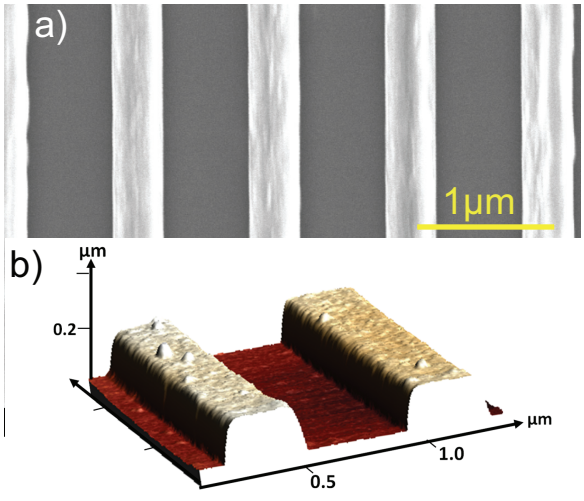

Figure 12. Top panel shows the scanning electron micrograph of AZO gratings formed by e-beam lithography and liff-off processes. Bottom panel shows the atomic force microscopy image of the gratings.[145]

by atomic layer deposition on a 3D polymer wood-pile structure. The deposition was conformal and produced smooth films that were plasmonic in the NIR wavelength range. Santiago et al.[149] studied electron-beam lithography of atomic-layer-deposited AZO films to fabricate plasmonic waveguide structures. It was found out that the grain size of the AZO film limits the smallest pattern that can be fabricated.

In addition to the methods above, TCO nanostructures can be synthesized as nanospheres and nanorods.[150–156] These oxide materials provide a number of viable chemical routes for synthesizing nanostructures, including the vapor-liquid-solid (VLS) technique, solution processing and many other techniques. These materials may also be functionalized with many different biomolecules, similar to the case with gold nanoparticles, which are commonly used in plasmonic enhanced biodetection schemes.[157–159] Recently, a number of studies have demonstrated LSPR behavior in TCO nanoparticles. These reports have also demonstrated tuning of the LSPR frequency by adjusting the doping level in the TCO nanoparticles. Kanehara et al.[160] have demonstrated that the SP resonance frequency in ITO nanoparticles could be tuned from a wavelength of about 1.6 μm to 2.2 μm by varying the doping. Doping of 10 mole% tin in indium oxide provided the shortest resonance wavelength of 1618 nm. Garcia et al.[161] demonstrated a tunable LSPR in ITO nanoparticles with sizes varying between 4 nm and 12 nm. The tunablility in the LSPR was achieved by varying the carrier concentration or by doping electrochemically. The application of a voltage from 1.5 to 4 V to the electrochemical cell caused a threefold change in the carrier concentration, which in turn caused a shift in the resonance wavelength. Similar work was reported with AZO nanoparticles where the doping concentration in the particles was changed not dynamically but chemically during the synthesis procedure.[162] This produced a shift in the LSPR spanning the wavelength range from 3 to 10 μm corresponding to doping levels from 7.3 to 1.4 atomic percent. Another work on ITO nanorod arrays was reported recently by Li et al.[163] In this work, ITO nanorods were grown on lattice-matched substrates with either controlled periodicity or random order. Both structures showed two plasmonic resonances corresponding to the axial and radial plasmonic modes excited in the nanorods, and these resonances were tuned by changing the annealing conditions. The carrier concentration in ITO can be increased by annealing in a nitrogen-rich ambient, which results in more oxygen vacancy defects that act as electron donors. In this way, changing the annealing conditions changed the carrier concentration and, hence, the permittivity of the ITO nanorods, which resulted in a shift in the plasmon resonance wavelength.

Transparent conducting oxides can be used not only as tunable plasmonic elements, but also as chemical sensors.[164] Recently, ITO films were shown to be useful as plasmonic gas sensors. Mishra et al.[165] demonstrated a surface plasmon resonance (SPR)-based hydrogen gas sensor by coating an ITO thin film on the core of an optical fiber. In another similar demonstration, Mishra et al.[166] showed an SPR-based ammonia sensor using ITO/aniline films.

Transparent conducting oxides have also been shown to support SPPs at the interface of a dielectric material. A thin film of ITO deposited on a prism was able to support SPPs when infrared light was incident in the Kretschmann geometry (schematic shown in **Figure 13**a).[167–171] Figure 13b–e shows the reflectivity measurements from prism coupling measurements reported by various groups. Figure 13b shows our results of prism coupling measurements on AZO, GZO and ITO films.[145] The reflectivity upon TM incidence at wavelength of 1548 nm shows dip due to the excitation of SPPs. All three TCO films possess their $\varepsilon' < -2$ at this wavelength. Reports of SPP excitation on AZO and GZO films are hardly found. However, SPPs on ITO film have been reported previously. Rhodes et al.[170] reported SPP excitation on ITO films in the NIR. Figure 13c plots the differential reflectivity versus incidence angle as reported in this article. The dips in the curves in the range of 47–63° correspond to the excitation of SPP. Noginov et al.[171] also report SPP excitation on ITO films using prism coupling geometry. Figure 13d shows the reflectance measurements reported in this article. The dips in the reflectance confirm SPP excitation on ITO films in the NIR. Many other TCOs such as F-doped tin oxide (FTO), zinc-indium-tin oxide (ZITO) and indium-doped cadmium oxide (ICO) can also support SPPs in the NIR.

Recently, we showed that TCOs are promising plasmonic materials for metamaterial applications in the NIR.[172] A stack of sub-wavelength thin, alternating planar layers of AZO and ZnO exhibited strong uniaxial anisotropy in the effective medium limit. The ZnO material is a dielectric with a permittivity of about 4. In contrast, AZO exhibited metallic properties in the NIR for wavelengths longer than about 1.8 μm. A metal/dielectric alternating layer stack can exhibit such strong anisotropy that the effective permittivity tensor can possess opposite signs in different directions. Such metamaterials can have many unusual properties, including the ability to exhibit negative refraction. Negative refraction may be observed only in low-loss metamaterials because high losses result in negligible transmittance and optical properties that are not suitable for negative refraction. Most of the noble metal-based devices in planar geometries suffer from high losses in the NIR. However, the AZO/ZnO combination overcomes this drawback by eliminating lossy noble metals and, thus, enabling a low-loss metamaterials in the NIR. We observed negative refraction in this medium using a standard experimental technique.[73] We also reported the figure of merit of this device to be about 11 at a wavelength of 1.8 μm, which is the highest value for any such device demonstrated in the NIR regime. This demonstration using AZO is an example of the efficacy of TCOs as plasmonic materials in metamaterial designs operating in the NIR. Similar demonstrations could be possible using ITO or GZO at the telecommunication or shorter wavelengths. There are many advantages of incorporating TCOs in such metamaterials other than low losses: a single material system could enable epitaxial growth of a superlattice. This can further lower the losses due to the crystalline structure of the individual layers. A single material system has advantages in fabrication and patterning. TCOs could also enable an important class of tunable metamaterials. ZnO-based TCOs can be useful in non-linear and active metamaterials because ZnO is known to exhibit a high second-order optical nonlinearity.[173,174]

Transparent conducting oxides have also been shown to be good for tunable plasmonic devices such as modulators and

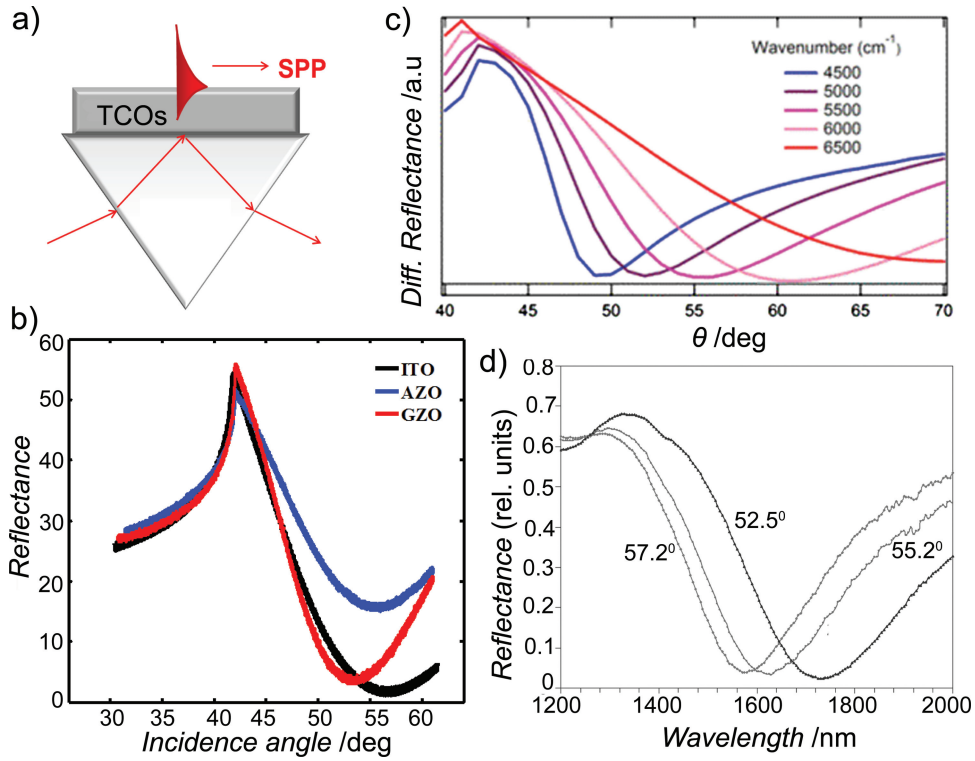

Figure 13. SPP excitation in TCO films using Kretschmann geometry. a) Schematic of the experimental set-up for prism coupling excitation of SPPs on TCO thin film. b) Reflectance measured at the excitation wavelength of 1548 nm upon TM incidence for PLD grown AZO (2 wt%), GZO (6 wt%) and ITO (10 wt%) films. c) Reflectance change measured on ITO film as a function of incidence angle for many different incident wavenumbers. Reproduced with permission.[170] Copyright 2006, American Institute of Physics. d) Reflectance of ITO film measured at three different angles of incidences: 57.2, 55.2 and 52.5°. Reproduced with permission.[171] Copyright 2011, American Institute of Physics.

switches. In particular, ITO and In-doped ZnO (IZO) demonstrated refractive index changes on the order of one in the visible range when subjected to external electrical fields.[175] In these demonstrations, a capacitor was formed by sandwiching 300 nm of a TCO film and 100 nm of silicon oxide between two gold layers. Applying a voltage across this capacitor can produce an accumulation of carriers at the TCO/silicon oxide interface. A thin (5 nm) layer accumulates electrons at the interface and thereby exhibits a refractive index change on the order of one at visible frequencies. Such a huge change in the index could be useful in demonstrating electric-field gated modulators and switches. Melikyan et al.[176] reported an SPP absorption modulator based on this field-effect tuning of the plasmonic properties of ITO. Their design, which was presented for the telecommunication wavelength, predicts a 12 dB modulation depth of the signal achieved in a 0.5 μm length of the plasmonic waveguide. A proof-of-concept device was fabricated and showed modulation of the plasmonic signal through the waveguide produced by an electric field acting on a 10-nm thick region of ITO. This fabricated device showed high insertion losses and low modulation depth, however. By further optimizing the device design, Babicheva and Lavrinenko proposed an improved device which shows low insertion loss and better modulation depth.[177] Stripes of TCO as an active layer was predicted to perform better in the modulator than a thin film. Another design was proposed by Lu et al.[178] based on a slot waveguide structure with much smaller insertion losses. In this case, a 10-nm-thick AZO layer sandwiched in the slot waveguide was proposed for field-effect tuning. The design predicts an insertion loss of less than 2 dB and a modulation depth of about 20 dB μm^{-1} at an operating wavelength of 1350 nm. Clearly, TCOs are promising materials for tunable/switching applications because thin layers of these materials can be switched from dielectric to plasmonic behavior by the application of moderate electric fields. Electrical control, a large change in the optical properties, and operation in the NIR (particularly at the telecommunication wavelength) makes TCOs attractive for active plasmonics and metamaterial devices.

To summarize, TCOs have been shown to be good alternatives to noble metals for plasmonic and metamaterial application in the infrared and NIR wavelength ranges. Transparent conducting oxides have great potential for enabling high performance, tunable, semiconductor compatible plasmonic and metamaterials devices.

5.5. Other Oxides and Sulfides

The popular TCOs based on indium oxide and zinc oxide are examples of a larger family of TCOs. There are many other compounds such as heavily doped CdO, ternary oxides such as $CdSb_2O_6$, $GaInO_3$, $MgIn_2O_4$, and perovskite oxides such as

$SrTiO_3$, $SrSnO_3$, Cd_3TeO_6, $BaSnO_3$ and $SrGeO_3$. Other than TCOs, there are non-stoichiometric oxides such as In_2O_3, TiO_2, IrO_2 and metallic VO_2 that are intrinsically doped. All of these materials can support large carrier concentrations ($> 10^{19}$ cm^{-3}) to provide Drude metal-like behavior. However, the low losses and the largest carrier concentrations have only been reported in doped ZnO and ITO. Nevertheless, there are some advantages offered by less-popular TCOs. For example, perovskite oxides show magnetoresistance properties that cannot be obtained in AZO or ITO.[179] Vanadium dioxide shows a metal-semiconductor transition at temperatures smaller than 100 °C, which can be useful in switching applications.[180,181] Hence, there are niche applications in which these materials can be very useful as plasmonic components. Recently, an infrared superlens formed by the perovskite oxides $SrTiO_3$, $BaFeO_3$ and $PbZrO_3$ was realized.[182] In this demonstration, the plasmonic properties of these materials arise not from free carriers, but from polaritonic resonances. When heavily doped perovskites can exhibit plasmonic properties in the NIR.

There are many non-stoichiometric semiconducting materials that are intrinsically doped heavily by defects or variations in the oxidation state. A recent demonstration of tunable plasmonic properties in $Cu_{2-x}S$ quantum dots is an example where Cu (II) acted as a p-type dopant in Cu_2S.[183] The doping was shown to be controllable in this case, and hence the plasma frequency was also adjustable. Interestingly, the LSPR modes in these quantum dots were actively tuned in the NIR range by controlling the exposure to oxygen ambient. A similar demonstration using tungsten oxide nanorods showed tunable LSPR modes in the NIR.[184] More recently, Wang et al.[185] demonstrated plasmonic properties in RuO_2 films in the NIR and in the long-wavelength edge of the visible spectrum. Both single crystal and polycrystalline films of RuO_2 were studied, and SPP excitation was confirmed using the Kretschmann geometry.

There are many more materials in this family that can exhibit metal-like plasmonic properties in different wavelength ranges. Hence, the possibilities of finding new plasmonic materials with improved performance and/or novel functionalities that could enable exciting plasmonic and metamaterials application are vast.

5.6. Summary

In this section, we considered the approach of turning semiconductors into plasmonic materials by doping them heavily. Many different semiconductor systems were considered: silicon, germanium, III–V materials, TCOs, perovskite oxides and non-stoichiometric oxides and sulfides. A short review of the developments in using semiconductors as plasmonic materials was also presented. We pointed out possible future directions and challenges in achieving plasmonic properties in new materials. This discussion is intended to serve only as a guide for many exciting explorations awaiting in this new field of semiconductor-based alternative plasmonic materials.

6. Metals to Dilute Metals

Another approach to decrease the excessive optical losses in metals is to reduce the carrier concentration in the material. A smaller carrier concentration may be achieved in intermetallic or metallic compounds, which we will term "dilute metals" in this work. In general, introducing non-metallic elements into a metal lattice reduces the carrier concentration. This also alters the electronic band structure significantly and might result in undesirable consequences, such as large interband absorption losses and higher Drude-damping losses. However, there is a lot of room for optimization, and this direction of research has yet to receive much attention from researchers. There are many advantages of plasmonic intermetallic or metallic compounds such as tunability and ease of fabrication and integration, which could out-weigh the disadvantages of these materials. Thus, it is worth pursuing a search for materials that are dilute metals.

A survey of the literature shows that the optical properties of many different classes of less-metals have been studied previously. Among them are metal silicides and germanides, ceramics such as oxides, carbides, borides and nitrides, which were all found to exhibit negative real permittivities in different parts of the optical spectrum.[24,75,76] Apart for these metal-nonmetal compounds, many intermetallics such as binary compounds of noble metals and transition metals, noble-alkali compounds and ternary compounds of metals are known to provide metallic optical properties.[75,186,187] None of these materials possess all the desirable properties, and in particular none of them exhibit low optical losses. However, we will focus on materials that are important from the view point of technological applications. Hence, we mostly focus on silicides, germanides and metal nitrides which are already used in silicon CMOS technology. A more general overview of intermetallic compounds for plasmonic applications is provided by Blaber et al.[75] In this review, we will provide a general approach towards finding better alternatives to gold and silver, and point out promising directions for future work.

6.1. Silicides and Germanides

Silicides and germanides are compounds of metals with silicon and germanium, respectively. These are non-stoichiometric compounds with large free carrier densities, which give them high DC conductivities. Many of these materials exhibit metallic optical properties spanning the MIR and NIR ranges.[97,188,189] The optical losses are not small because of interband transition losses and large carrier relaxation rates. However, there are possibilities for optimizing the material composition, which might reduce the losses. These materials are technologically important because of their current use in standard silicon CMOS integrated circuits–silicides and germanides are used in the salicide process to form contacts to the active regions in CMOS devices.[190,191] Many of these materials also grow epitaxially on silicon. Thus, these materials are very advantageous from the perspective of standard fabrication and integration.

Silicides and germanides can be grown by many different deposition techniques.[192–194] Depositing a thin layer of metal on silicon or germanium and heating the structure to high temperatures would grow silicide or germanide layers at the interface of the metal and the silicon or germanium. Co-deposition of metal and silicon/germanium followed by high-temperature

annealing also produces silicides/germanides. The high-temperature annealing could be accomplished either by a slow furnace annealing or by rapid thermal processing. Chemical vapor deposition is another technique that has been adopted to produce these materials. Physical vapor deposition techniques such as sputtering and pulsed laser deposition[195] have also been used to grow good-quality silicides and germanides. In addition, many silicides have can be grown as epitaxial films on silicon (111) and (100) substrates,[196,197] and a few germanides can be grown as epitaxial films on crystalline germanium substrates.[198,199] Solid-phase epitaxy is also a common technique used to grow such crystalline films of silicides and germanides. Clearly, the technology to grow and deposit thin films of silicides and germanides is mature, and the techniques to pattern and etch these thin films are also well-understood. Silicides and germanides can be etched by both wet and dry etching techniques.[200–202] Fluorine plasma etching possesses good characteristics for these materials. In addition, lift-off techniques are also available for silicides and germanides, and hard masks such as silicon oxide or nitride are common. In this process, the semiconductor substrate is first patterned with silicon oxide or nitride, followed by the deposition of metal. This is followed by a high-temperature annealing treatment and a metal etch process. During the annealing, a silicide or germanide film is formed only in the regions where the metal is in contact with semiconductor and not on the silicon oxide or nitride layer. Subsequent metal etching removes the unreacted metal, leaving a silicide or germanide film in the regions not covered by the oxide/nitride. This technique is commonly used in the salicide process.

The properties of various transition-metal silicides have been studied widely. Murarka[192] provides a review of silicides for electronic applications, and there are many reports on the optical properties of silicides. Various silicides formed from metals such as Co, Cr, Fe, Hf, Ir, Nb, Ni, Os, Pt, Pd, Re, Rh, Ru, Ta, Ti, V, W, Zr, Ca, Mg and alkali metals have been studied.[203] The dielectric functions of these silicides show metallic behavior in the MIR, NIR and visible ranges. The losses are quite high in these materials due to interband transitions in the regions where their real permittivities are small in magnitude. Comparing to noble metals, silicides exhibit very high losses.[75] While they are useful in the longer wavelengths where there are no interband transitions, their real permittivity values are large in magnitude, similar to noble metals. Nevertheless, the manufacturing advantages of silicides make them promising materials for infrared plasmonics. Recently, Soref et al. proposed using $PdSi_2$ as plasmonic material for MIR plasmonics[204] and Cleary et al. demonstrated an application of silicides for an SPP-based infrared biosensor where $PdSi_2$ was used as a plasmonic material.[205] Also, Blaber et al. provided a brief review of silicides for plasmonic applications.[75] Notably, the calculated quality factors for LSPR applications are high for some silicides such as $TiSi_2$.

There are many reports on the properties of germanides formed with metals such as Ru, Os, Ba, Sr, Ca, Mg, Cr and other rare earth metals and alloys.[206–210] While many rare-earth germanides are semiconducting with a broad range of bandgap values, some transition-metal germanides are also known to be metallic.[211,212]

6.2. Interstitial Metal Nitrides

Metal nitrides such as titanium nitride, zirconium nitride, tantalum nitride and hafnium nitride exhibit metallic properties in the visible and longer wavelengths.[76,213] These are non-stoichiometric, interstitial compounds with large free-carrier concentrations. These materials are also refractory, stable and hard and allow for tuning of their optical properties by varying their composition. Technologically, they are important because many of them are currently used in silicon CMOS technology as barrier layers in copper-Damascene processes[214] and as gate metals to n-type and p-type transistors.[215] Titanium nitride is usually used as the barrier layer in the dual Damascene process.[216] Thus, metal nitrides offer fabrication and integration advantages which could be useful in integrating plasmonics with nanoelectronics.

Refractory metal nitrides can be deposited by many techniques such as chemical vapor deposition (CVD);[217] atomic layer deposition (ALD);[218] physical vapor deposition (PVD) such as reactive sputtering,[213] pulsed laser deposition[219,220] and ion-assisted reactive evaporation;[221] and wet-chemical techniques.[222–225] Because of their very high mechanical strength and very high melting temperatures, PVD techniques such as evaporation or sputtering directly from a nitride source are difficult for these materials. Instead, a metal source is more commonly used for sputtering or laser ablation with nitrogen as a reactive gas. More common are CVD techniques, and various metal sources are used for such processes. Metal-organic-CVD is employed quite often due to the availability of many low-vapor-temperature metallo-organic sources. Wet-chemical synthesis of these metal nitride nanostructures is also difficult because commonly used protic solvents that contain hydroxyl groups are not preferable. Hydroxyls involved in the reaction during the synthesis could produce oxides or oxynitrides rather than nitrides. Thus, solution-processing techniques using aprotic or non-polar solvents such as benzene are necessary to produce metal nitride nanoparticles or thin films.[225] A common approach to circumvent this requirement is to produce oxide nanostructures via solution-processing techniques and to subsequently nitridize the resulting nanostructures by techniques such as ammonia annealing.[226] Each of these approaches has its own advantages and disadvantages. More commonly, thin films are grown by reactive sputtering and CVD, whereas nanoparticles are grown by nitridation and solution processing techniques.

Many of these nitrides can be grown epitaxially on various substrates, including Si(100). In addition, HfN, TiN, TaN, and ZrN have cubic lattices and can be grown epitaxially on cubic substrates such as MgO.[227–230] Some nitrides such as TiN can also be grown as psuedomorphic epitaxial layers on c-sapphire substrates.[231] On silicon substrates, many of the cubic rock-salt nitrides grow as domain-matched epitaxial layers.[232] Epitaxial growth allows the growth of ultrasmooth and ultrathin films. This is very important for plasmonic applications where noble metals perform very poorly and where thin, high-quality films with low losses are desirable.

Reports on the optical properties of many of these nitrides are scarce. However, there are only a few studies that describe the optical properties, SPP characteristics and LSPR properties

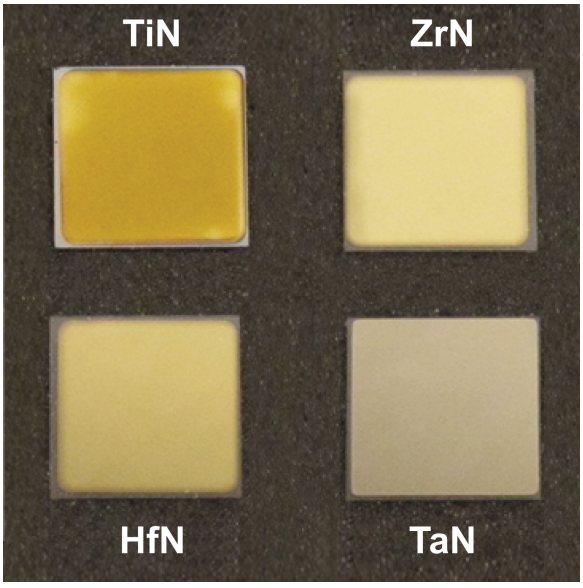

Figure 14. Optical image of thin films of metal nitrides deposited on glass substrates. The films were deposited by DC reactive sputtering. The thickness of films is in the range of 100 to 120 nm. The metallic luster indicates the possibility of plasmonic behavior in the visible spectrum. The color of the films correlates with the plasma frequency or carrier concentration in these films.

of some of these metal nitrides. Since metal nitrides exhibit a metallic luster (see **Figure 14**), their dielectric functions could exhibit metallic properties in the visible spectrum. Hence, we recently studied the optical properties of titanium nitride, tantalum nitride, hafnium nitride and zirconium nitride.[76] **Figure 15** shows the dielectric functions of thin films of these metal nitrides deposited by DC reactive sputtering. The dielectric functions were retrieved from the spectroscopic ellipsometer measurements on a thin film sample. The Drude-Lorentz model parameters of these metal nitrides extracted from ellipsometry measurements are listed in Table 2. Except titanium nitride, the nitrides were deposited in nitrogen-deficient ambient, which would result in metal-rich films. When the composition of sputtering ambient was varied from 100% nitrogen to 20% nitrogen and 80% argon, all the metal nitrides except titanium nitride exhibited optical properties that changed from dielectric behavior to metallic behavior. Titanium nitride shows a lower carrier concentration under nitrogen-rich deposition conditions. However, the metallic property in TiN is not lost because the change in the carrier concentration is small. It is also important to note that most of these nitrides have larger carrier relaxation rates than those of the noble metals, which increases the optical losses in these nitrides. Additionally, interstitial nitrides exhibit interband transition losses in the visible and ultraviolet ranges. Thus, their optical properties are undesirable in these ranges unless significant growth-parameter optimization is employed. The deposition conditions can change the Drude relaxation rate, the plasma frequency and the strength of the interband transitions. For example, TiN films deposited at two different temperatures exhibit different optical properties. Table 2 shows that the plasma frequency is lower in the case of TiN films deposited at 500 °C than that of the films deposited at 800 °C. Also, the Drude relaxation rate is higher in the case of films deposited at lower temperature. Thus, careful optimization of the deposition conditions is necessary to achieve a low-loss TiN film.

The plasmonic properties of interstitial metal nitrides have been examined by electron-energy-loss-spectroscopy (EELS). When a monochromatic beam of high energy electrons pass through a thin film, the electrons suffer energy loss due to various mechanisms occurring in the thin film. One of the relevant phenomena is to lose energy to surface plasmons on metallic thin films. Thus, EELS measurement can provide information about plasmon energy, effective masses of charge carriers, and interband transition energies and strengths. EELS studies have been reported on many nitrides including TiN,

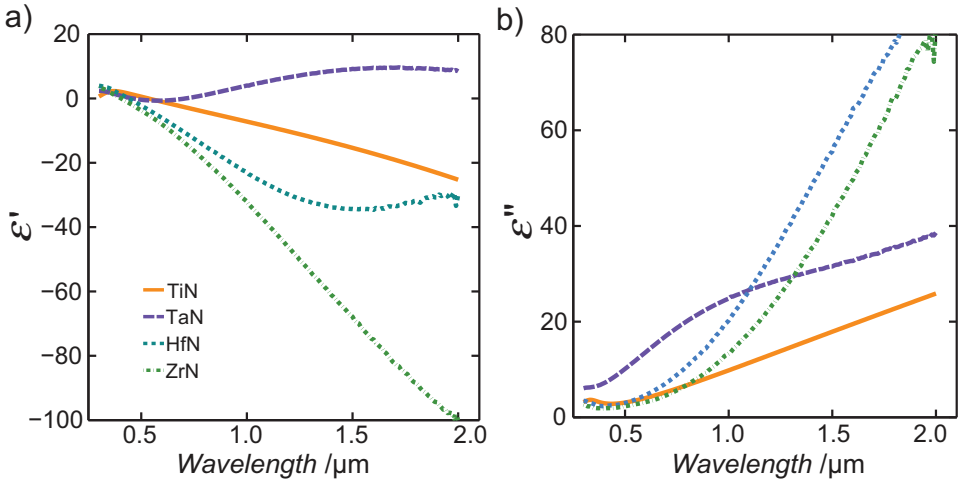

Figure 15. The real (a) and imaginary (b) parts of dielectric functions of metal nitride plasmonic materials extracted from spectroscopic ellipsometry measurements. Reprinted with permission.[76] Copyright 2011, Optical Society of America.

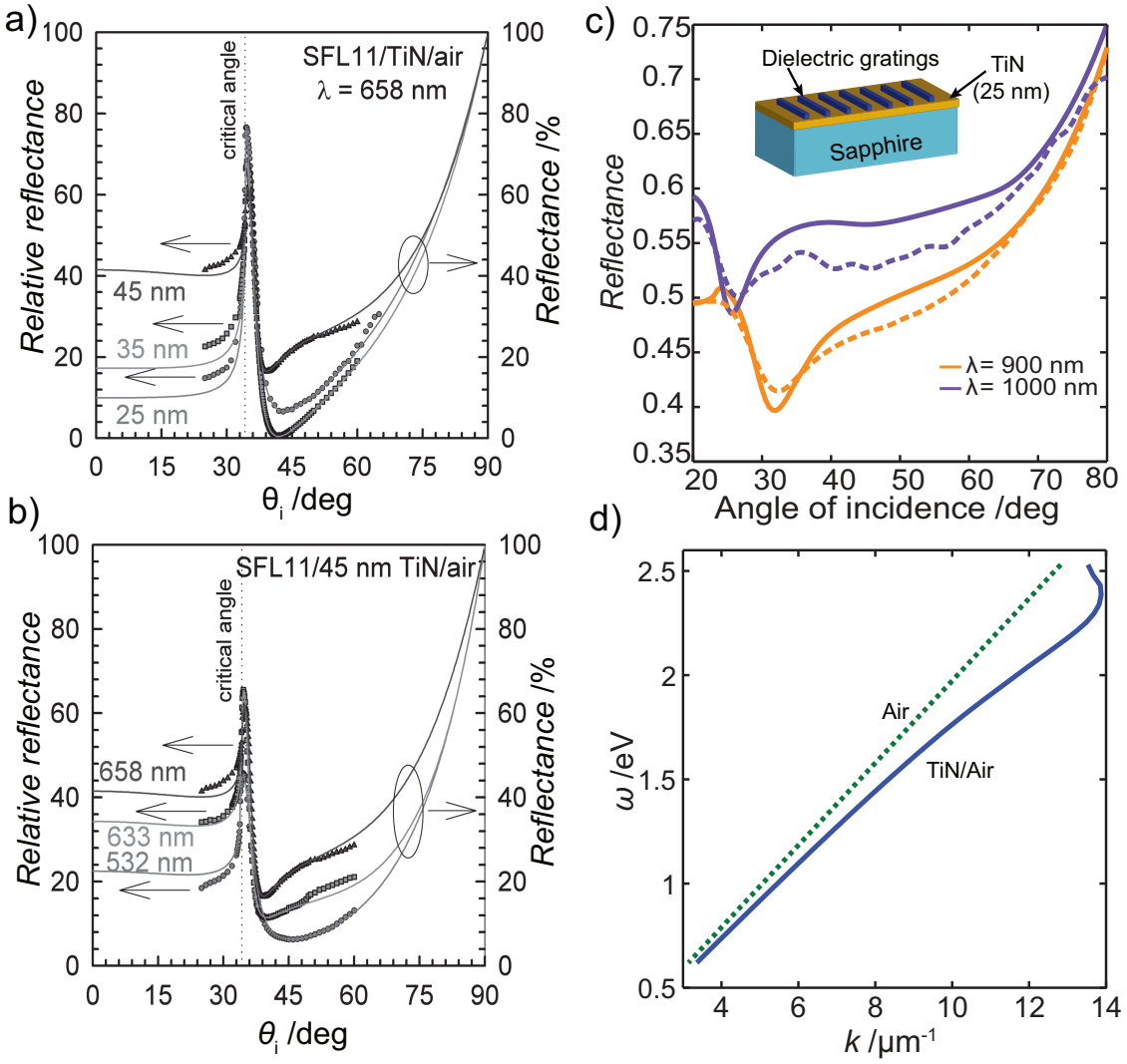

Figure 16. Reflectance of TiN films of thickness 25, 35 and 45 nm incident by 658 nm wavelength (a), and 45 nm TiN film incident by 658, 633 and 532 nm wavelength sources (b), as measured by Chen et al. using prism coupling geometry. The dips correspond to the excitation of SPPs. a,b) Reproduced with permission.[242] Copyright 2011, American Institute of Physics. Angular reflectance from dielectric gratings fabricated on top of 25 nm thick TiN film (c). The inset shows the sample schematic. The measured and calculated reflectances show dips in the angle range of 20–35°, which correspond to the excitation of SPPs on the TiN film. c) Reproduced with permission.[231] Copyright 2012, Optical Society of America. Dispersion curves for air and TiN/air interface (d). At photon energy of about 1.2 eV, the gratings provide exact additional momentum to excite SPPs on the TiN film when the incident angle in the range 20–35°.

TiAlN, TaN, ZrN, Zr_3N_4, YN, VN, NbN, Cu_3N and WN.[233–239] Most of these materials exhibit metallic properties with a large plasma frequency when metal-rich, while nitrogen-rich films show dielectric properties with large interband losses in most of the cases. The previous studies on these materials also mention that metal-rich nitrides can support both bulk plasmons and surface plasmons. However, reports on SPP excitation are available only for titanium nitride films. Steinmüller-Nethl et al. demonstrated SPP excitation on an approximately 30-nm-thick TiN film deposited by sputtering.[240] In that study, SPP excitation was demonstrated at wavelengths of 700, 750, 800 and 850 nm. Hibbins et al. extended this work to many wavelengths in the range from 500 to 900 nm.[241] In addition, SPPs were coupled onto TiN thin film via gratings that were created by depositing a TiN film on a patterned substrate. Grating-coupled SPP excitation on metal films is one of the popular techniques to extract the dielectric functions of optically thick metal films. Hibbins et al. adopted this technique to retrieve the dielectric function of a 600-nm-thick TiN film deposited by magnetron reactive sputtering. Recently, Chen et al. demonstrated SPP excitation on TiN films in the visible wavelengths using the Kretschmann geometry.[242] TiN film was deposited on sapphire substrate and mounted on a prism to excite SPPs by attenuated total internal reflection. The results of their measurements are shown in **Figure 16**a and b. Figure 16a shows the reflectance measurements on TiN films of different thickness with excitation fixed at 658 nm wavelength. Figure 16b shows the reflectance of 45 nm thick TiN film at different excitation

wavelengths. The dips in the reflectance confirmed SPP excitation. In our recent studies on TiN films, we also reported SPP coupling on epitaxial TiN thin films deposited by DC reactive sputtering on c-sapphire substrates.[231] The SPP modes were coupled onto the TiN film using a dielectric grating coupler formed by patterning a thin layer of polymer (electron-beam resist, ZEP-520A) on top of the TiN film. A schematic of the experimental set-up is shown in the inset of Figure 16c. Figure 16c also shows the angular reflectivity measured at wavelengths of 900 and 1000 nm. The dips in reflectance correspond to SPP excitation, which was also verified by numerical calculations. The fact that the SPP coupling condition was satisfied at the measured reflectance dips is also verified by the dispersion curves plotted in Figure 16d.

When patterned, titanium nitride has also been shown to exhibit LSPR modes. Cortie et al. sputter-deposited TiN on a monolayer of self-assembled polystyrene spheres.[243] This produced TiN-capped, 200-nm-diameter dielectric spheres, which were predicted to exhibit a plasmonic resonance near an excitation wavelength of 900 nm. However, the measurements did not show a distinct resonance peak as expected, probably because the TiN-capped spheres were not isolated from each other. The authors mentioned that the high loss in the TiN material is the reason for not observing appreciable resonance peak, but Mie theory-based analyses by Guler et al. showed that the LSPR mode in TiN nanospheres is comparable in strength with that in gold nanospheres.[244]

6.3. Summary

Many classes of materials such as intermetallics and ceramics exhibit plasmonic behavior in the optical range. However, none of them exhibit optical properties better than those of silver. Nevertheless, some materials such as TiN have optical properties similar to gold. There is, however, a great promise in optimizing the properties of these materials. The important development towards the design of better plasmonic materials could come from the theoretical domain. For example, a binary metal nitride system such as $Ti_xZr_{1-x}N$ might exhibit better optical properties than either TiN and ZrN. Further studies in this direction are therefore essential for finding better plasmonic materials.

7. 2D Plasmonic Materials

Recently, plasmonics with 2D materials, or flatland plasmonics,[245–249] has gained much attention, especially after the demonstration of plasmons in graphene.[250–253] Two-dimensional materials such as graphene have many advantages over bulk 3D materials from both scientific and technological perspectives.[249] The optical properties of 2D materials are quite different from those of bulk, 3D materials, which results in significantly different plasmon dispersion relationships.[254,255] Two-dimensional materials are technologically important because their properties are useful in many other applications, including electronics.[249,256–261] The properties of 2D materials can be dynamically tuned by electrical, chemical, electrochemical and other means.[262,263] For example, the optical properties of graphene can be tuned by electrical field-effect methods.[250–253,264–266] In addition, 2D materials can be processed via conventional, planar fabrication techniques.[267,268] Currently, the synthesis of large-area single, crystalline 2D materials is a challenge that limits the set of suitable applications for these materials.[269,270] However, there is now significant effort invested in overcoming this bottleneck.

There are reports of the observation of 2D electron gas (2DEG) systems in semiconductor inversion layers,[271] semiconductor heterostructures,[272,273] polar interfaces of oxides,[274] and materials that grow as 2D sheets such as graphene,[275] many chalcogenides such as molybdenum disulphide,[259,263] perovskite materials and oxide nanosheets.[276] Plasmons have been observed on semiconductor inversion layers,[271] semiconductor heterostructures,[277] and graphene.[250,252,253] Except in the case of graphene, plasmons were observed in other cases only at low temperatures because of the high losses (low carrier mobility or high carrier scattering rates) occurring at room temperature. All of the observations of plasmons were made in the MIR or longer wavelength ranges. Plasmons in the visible or NIR ranges were not observed in any of these 2D materials because of insufficient carrier densities. In order to understand the behavior of plasmons in 2DEGs, consider the dispersion relation shown in Equation 7a:

$$\frac{n_S e^2}{\varepsilon_0 \varepsilon_S m^*} q_p = \omega^2 \left(1 + \frac{i\gamma}{\omega}\right) \tag{7a}$$

Here n_s is the surface charge density, ε_s is the permittivity of the surrounding medium, m^* is the carrier effective mass, γ is the carrier relaxation rate, and q_p is the plasmon wavevector. This equation is valid when $\gamma << \omega$ and for carriers with a parabolic band or carriers that have a non-zero effective mass. In the case of graphene, the carriers behave as if massless, and hence the dispersion relation is different. Equation 7b describes the plasmon dispersion relation in graphene at low temperatures:

$$\frac{e^2 E_F}{\pi \hbar^2 \varepsilon_0 \varepsilon_S} q_p = \omega^2 \left(1 + \frac{i\gamma}{\omega}\right) \tag{7b}$$

In this case, E_F is the Fermi energy of single-sheet graphene. In graphene, the carrier density is directly proportional to the square on E_F, and it thus can be computed from the knowledge of E_F alone. A carrier concentration of 3×10^{13} cm^{-3} corresponds to an E_F of about 0.64 eV.[278]

Equations 7a,b allow us to quantitatively examine the characteristics of plasmons in 2D plasmonic materials. One of the important characteristics is the ratio of the free-space wavelength (λ_0) to the plasmon wavelength (λ_p). Another important parameter is the number of plasmon wavelengths the plasmon wave will propagate, which is given by $\mathrm{Re}(q_p)/\mathrm{Im}(q_p)$. From Equation 7a,b, we can deduce these quantities as shown in Equation 8. For parabolic-band 2DEGs:

$$\frac{n_S e^2}{c\ \varepsilon_0 \varepsilon_S m^*} \left(\frac{\lambda_0}{\lambda_p}\right) = \omega, \quad \frac{\mathrm{Re}(q_p)}{\mathrm{Im}(q_p)} = \frac{\gamma}{\omega} \tag{8a}$$

and for the case of massless carriers as in graphene:

$$\frac{e^2 E_F}{c\ \pi \hbar^2 \varepsilon_0 \varepsilon_S} \left(\frac{\lambda_0}{\lambda_p}\right) = \omega, \quad \frac{\mathrm{Re}(q_p)}{\mathrm{Im}(q_p)} = \frac{\gamma}{\omega} \tag{8b}$$

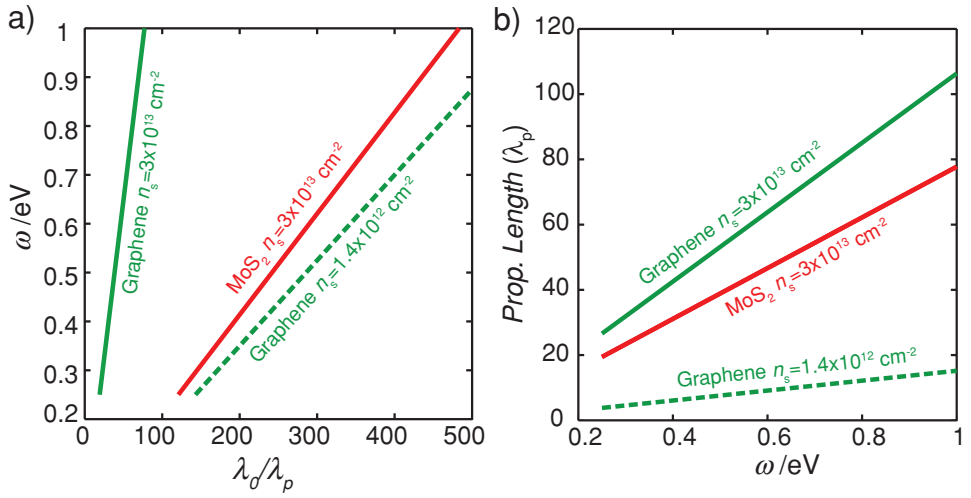

Figure 17. Plasmon characteristics on two-dimensional electron gas systems: graphene and semiconducting MoS_2. a) shows the dispersion curves for a particular carrier concentration (n_s) in MoS_2 and two different n_s in graphene. On the x-axis is plotted the quantity λ_0/λ_p, which is the ratio of free-space wavelength (λ_0) to the plasmon wavelength (λ_p). b) Plots the calculated propagation length (in number of plasmon wavelengths) for the two materials. The parameters for this simplified calculations were obtained from refs.[259,278]

Note that plasmons can exist in 2DEGs at all wavelengths. However, the plasmon wavelength might be too short to enable either excitation or observation of the plasmon mode. Also, when the plasmon wavelength shrinks below a few nanometers, non-local effects, which are ignored in the equations above, will have to be considered. Thus, practical considerations limit the plasmon wavelength (λ_p) to not more than a few hundred times smaller than the free-space wavelength (λ_0). In **Figure 17**a we plot this quantity, λ_0/λ_p, for graphene and for a typical 2D semiconductor such as MoS_2 ($m^* = 0.45$) for two different carrier densities. Figure 17b shows the quantity $\mathrm{Re}(q_p)/\mathrm{Im}(q_p)$, which is essentially the number of plasmon wavelengths that the plasmon wave will propagate in the material. In this plot, graphene is assumed to have a DC mobility of 10 000 $cm^2\ V^{-1}\ s^{-1}$ with a carrier scattering rate assumed constant, $\gamma = 1/(7\times10^{-14})\ s^{-1}$ for $n_s = 3\times10^{13}\ cm^{-2}$ and $\gamma = 1/(1\times10^{-14})\ s^{-1}$ for $n_s = 1.4\times10^{12}\ cm^{-2}$. More details and precise calculations are provided by Jablan et al.[278] The parameters for MoS_2 are computed from the DC mobility report of 200 $cm^2\ V^{-1}\ s^{-1}$ and effective mass of 0.45.[259] Unlike graphene, interband transitions in MoS_2 are absent for both carrier concentrations in the spectrum displayed in the figure. The effect of optical phonons in MoS_2 is also not included in this plot. We note that a high carrier concentration is required in order to observe plasmons in the MIR range. Plasmons in the NIR and visible ranges are very hard to observe with carrier concentrations lower than $1\times10^{14}\ cm^{-2}$. MoS_2 requires an even higher carrier concentration than graphene because of its large effective mass. In Figure 17a, the curve for MoS_2 with $n_s = 1.4\times10^{12}\ cm^{-2}$ is out of scale, and the curve for $n_s = 3\times10^{13}\ cm^{-2}$ shows that the plasmon wavelength is about 100 to 200 times smaller. On the other hand, graphene accomplishes this behavior for a carrier density of an order of magnitude lower. When comparing the losses or propagation length shown in Figure 17b, graphene performs much better owing to its high carrier mobility. The actual propagation length in graphene would be about a few tenths of the free-space wavelength for $n_s = 1.3\times10^{12}\ cm^{-2}$, whereas the same in MoS_2 would be about a hundredth of the free-space wavelength for the same carrier density. The conclusions drawn here for MoS_2 may be generalized to any other 2D semiconductor material. It is preferable to have a small effective mass, a bandgap higher than the photon energy, and the possibility of a large carrier concentration. In this regard, the oxide interfaces and semiconductor heterojunctions now under development may be useful because of their ability to support higher carrier concentrations.[274,279,280] NIR or visible operation of these materials requires carrier concentrations in excess of $10^{14}\ cm^{-2}$, which is currently difficult to achieve in both graphene and other 2D materials.

8. Comparative Study

Recently, many new ideas have fused the fields of plasmonics and metamaterials, leading to a variety of new devices. Each of the proposed devices would have its own optimum operating condition. In general, the performance of the device is a function of its structure, geometry and material properties. For many standard device geometries, the performance can be estimated for a given set of constituent materials. Such estimations would allow us to evaluate how good or bad a particular material set is for the specific application. Thus, the performance of devices belonging to a particular class can be compared for different plasmonic materials.[24,281] In this work, we consider SPP waveguides, LSPR devices, negative index metamaterials (NIMs), TO devices such as cloaks and light concentrators, HMMs, and epsilon-near-zero applications. Similar analyses for other applications may be qualitatively extended from the comparative study presented here. Here, we restrict our analyses only to 3D or bulk plasmonic materials.

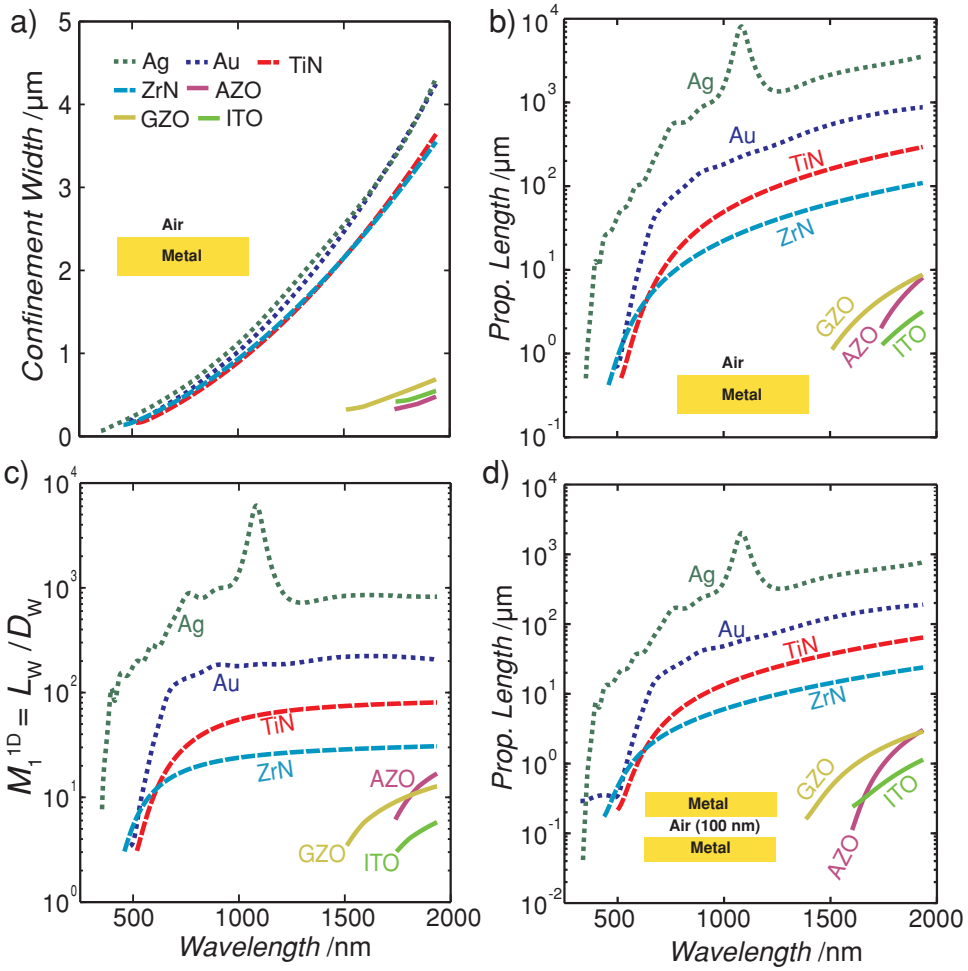

Figure 18. Comparative study of performances of various plasmonic materials in SPP waveguiding applications: a) field confinement width (D_W) of SPPs on plasmonic material/air interface (inset shows the geometry of the structure). b) $1/e$ propagation length (L_W) of SPPs along the plasmonic material/air interface. c) The figure-of-merit M_1^{1D} is defined as the ratio of propagation length (L_W) to confinement width (D_W) for SPPs on dielectric/metal interface.[283] This figure-of-merit is indicative of the trade-off offered by each plasmonic material between confinement and propagation length. d) Propagation length of long-range symmetric mode in metal/insulator/metal waveguide with 100 nm air as the insulator (the inset shows the geometry of the structure). The calculations for these plots use optical constants of noble metals from ref.[22]

8.1. SPP Waveguiding

Propagating SPPs along metal-dielectric interfaces may be guided using many different waveguide geometries (see Gramotnev and Bozhevolnyi[282] and references therein). One-dimensional geometries include a single metal-dielectric interface, metal-insulator-metal (MIM) and insulator-metal-insulator (IMI) designs. Two-dimensional waveguides include slot-, stripe-, V-groove and dielectric-loaded waveguide designs. Each of these designs offer different trade-offs between two important performance metrics: propagation length (L_w) and confinement width (D_w).[283,284] In order to get an insight into the trade-off between propagation length and confinement width, it is useful to plot these quantities for a single metal/dielectric interface. Consider a single interface of any of the plasmonic materials with air. The propagation length (L_w) and confinement width for SPPs propagating at the interface may be computed using Equation 9 and 10.[283]

$$L_w = 1/\left\{k_0\sqrt{\frac{\varepsilon_m}{\varepsilon_m+1}}\right. \tag{9}$$

$$D_w = \begin{cases} \delta_{air} & |\varepsilon_m| \geq e \\ \delta_{air} + \delta_m(1-\ln(|\varepsilon_m|) & |\varepsilon_m| < e \end{cases} \tag{10}$$

where $\delta_{air} = 1/\mathrm{Re}\left\{k_0\sqrt{\frac{-1}{\varepsilon_m+1}}\right\}$, $\delta_m = 1/\mathrm{Re}\left\{k_0\sqrt{\frac{-\varepsilon_m^2}{\varepsilon_m+1}}\right\}$, $k_0 = \omega/c$ and ε_m is the permittivity of the plasmonic material. **Figure 18** a,b plot the confinement width and propagation length for metal/air interface. TCOs provide good confinement, but very poor propagation length. TiN and ZrN also provide better

confinement than gold and silver. However, propagation length is smaller. We have shown that the SPP characteristics on TiN films resemble those on gold film when the Drude-damping in gold is artificially increased by 3.5 times.[231] Since thin gold films are known to exhibit higher losses, a loss factor of 3.5 may not be unreasonable.[45] Thus, TiN may be a good replacement to gold. The trade-off between propagation length and confinement width is conveniently captured by figure-of-merit (M_1^{1D}) defined as the ratio of propagation length to confinement width.[283] Figure 18c shows the figure-of-merit for 1D SPP waveguides plotted for different plasmonic materials. The trade-off is offered the best by silver, followed by gold, nitrides and TCOs. Nitrides and TCOs are less metallic compared to gold or silver. Hence, field penetration into these plasmonic materials is more than that in gold or silver waveguides. Since plasmonic components have losses, more field penetration causes more attenuation or less propagation of the SPPs. From the plot of M_1^{1D}, it may be inferred that the reduction in propagation length is dramatic for nitrides and TCOs in comparison to the improvement in field confinement. Thus, M_1^{1D} is smaller with nitrides and TCOs than with noble metals.

The trade-off between propagation length and confinement width offered by many different plasmonic materials may be fairly compared when one of the quantities is held constant. Here, we choose MIM waveguide with a fixed gap size providing a constant confinement width, and we compare the propagation lengths of the symmetric long-range SPP mode.[164,231] Figure 18d shows the propagation length of the long-range symmetric mode in a MIM waveguide with air as the dielectric and a gap size of 100 nm. A number of alternative plasmonic materials are used as the metallic part of the waveguide, as shown in the figure. We first note that TCOs exhibit poor propagation lengths compared to those of gold and silver. Titanium nitride, too, performs worse than either gold or silver. However, the propagation length in the titanium nitride waveguide is comparable to that of gold with a loss factor of 3.5. The zirconium nitride waveguide performs slightly better compared to the titanium nitride waveguide.

In general, for SPP waveguiding applications, the field penetration into the metal influences the trade-off between confinement and propagation loss significantly. A larger negative real permittivity gives rise to smaller field penetration into the metal, while a smaller imaginary permittivity leads to lower losses. Hence, the figure of merit would take the form $[\mathrm{Re}(\varepsilon_m)]^2/\mathrm{Im}(\varepsilon_m)$ where ε_m is the permittivity of the plasmonic material.[24] This quantity is plotted for different alternative plasmonic materials in **Figure 19**. Noble metals outperform all other materials because of their large negative real permittivity. The large negative real permittivity is a consequence of large plasma frequency or large carrier concentration. Since the figure-of-merit, $[\mathrm{Re}(\varepsilon_m)]^2/\mathrm{Im}(\varepsilon_m)$ exhibits stronger dependence on real permittivity than imaginary permittivity, having a larger plasma frequency results in a more significant improvement in performance than reducing the losses. Because all the alternative plasmonic materials we considered have lower plasma frequencies than noble metals, their performance metrics as SPP waveguides are worse than those offered by noble metals.

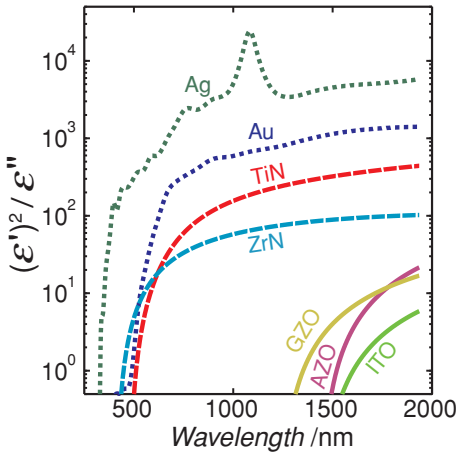

Figure 19. The performance of many 2D plasmonic waveguides, non-spherical LSPR structures, resonant metamaterial devices such as negative-index-metamaterials depend on the quantity $\frac{[\mathrm{Re}(\varepsilon_m)]^2}{\mathrm{Im}(\varepsilon_m)}$ (ε_m is the permittivity of plasmonic material). This quantity is plotted in the figure for various plasmonic materials.

8.2. LSPR Applications

The LSPR modes occurring in metal nanoparticles are useful in many applications such as sensing, catalysis and medical applications.[12,16] Metal nanoparticles at resonance show high field enhancement on the metal surface, which enhances the interaction of light with the local medium surrounding the nanoparticles. At resonance, the absorption cross-section (σ_{abs}) of the nanoparticles increases enormously and reaches a maximum. This causes the metal nanoparticles to strongly absorb light at the resonance and causes local heating, which is useful in catalysis and medical applications. In far field, the strength of resonance may be observed by extinction efficiency which may be characterized by extinction cross-section (σ_{ext}). Near-field enhancement, absorption cross-section and extinction cross-section are important quantities in assessing different plasmonic materials for LSPR applications. Using a dipole approximation in the electrostatic limit, the near-field enhancement, absorption cross-section and extinction cross-section of spherical plasmonic nanoparticles have been calculated previously for conventional and alternative plasmonic materials.[285] **Figure 20** plots the maximum field enhancement ($|E_{max}/E_0|$) on the surface of spherical nanoparticles of gold, silver, titanium nitride, zirconium nitride and TCOs.[164,231] **Figure 21**a and b plot normalized σ_{abs} and normalized σ_{ext} respectively for spherical nanoparticles of diameter $\lambda/10$. The refractive index of the host medium surrounding the nanoparticles is assumed to be 1.33. Clearly, silver outperforms all other materials with resonances in the blue part of visible spectrum. Other materials show comparable performance in different parts of the NIR and visible ranges. Notably, TCOs could enable LSPR applications in the NIR without the need for complex geometries such as core-shell structures. Titanium nitride and zirconium nitride have similar performance and exhibit LSPR modes in the visible part of the spectrum. In particular, titanium nitride could be of significant interest for biological applications because TiN is biocompatible[286] and its LSPR mode lies in the biological

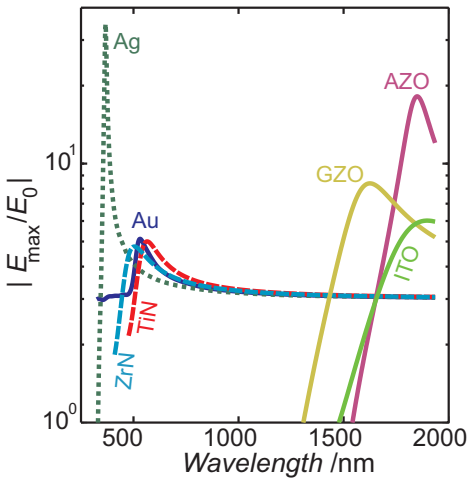

Figure 20. The maximum field enhancement on the surface of a spherical nanoparticle of the plasmonic material computed from quasistatic approximations. The nanoparticles are assumed to be in a host of refractive index 1.33.

transparency window (700–1000 nm).[287] Also, TiN may be useful in plasmonic heating applications[288] because TiN nanoparticles have large absorption cross-section at the plasmon resonance and TiN has extremely high melting point (>2900 °C).

When the particle geometry is more complex than a sphere, the LSPR wavelength and its strength change. In general, small spherical particles exhibit a resonance strength that is proportional to $\mathrm{Re}\{-\varepsilon_m\}/\mathrm{Im}\{\varepsilon_m\}$, where ε_m is the permittivity of the plasmonic material.[24] When the geometry changes from a sphere to cigar-like elongated structures, for example, the resonance quality varies as $[\mathrm{Re}(\varepsilon_m)]^2/\mathrm{Im}(\varepsilon_m)$. Alternative plasmonic materials have smaller magnitudes of real permittivity due to their smaller plasma frequencies, and hence they perform poorly when compared to noble metals for such complicated geometries.[289]

8.3. Negative-Index Metamaterials

Artificial magnetism is accomplished in metamaterials by introducing nanostructures that produce a tiny current loop upon optical excitation.[5,290] Current loops act like inductors producing magnetic response. In order to achieve negative index, both permittivity and permeability need to be negative.[290–293] A strong magnetic resonance can produce negative permeability and a strong electric resonance can produce negative permittivity. Overlapping electric and magnetic resonances in the nanostructured metamaterial enables negative index. Thus, NIMs are resonant devices which generally rely upon plasmonic resonances in the nanostructures that constitute them. The nature of the resonance in the metal-dielectric nanostructures is similar to that in LSPR modes. This makes the performance dependence the same as that of LSPR structures. We know from the previous section that for non-spherical geometry of the plasmonic nanostructures, the performance of the device scales as $[\mathrm{Re}(\varepsilon_m)]^2/\mathrm{Im}(\varepsilon_m)$, where ε_m is the permittivity of the plasmonic component. Hence, a large magnitude of real permittivity of metal boosts the performance significantly. In other words, a large carrier concentration in the metal makes a better negative-index metamaterial. Since alternative plasmonic materials have smaller carrier concentration than in noble metals, their magnitudes of real permittivity are smaller than those of noble metals. Hence, the alternative plasmonic materials that we considered do not perform as well as noble metals for NIM applications. A detailed analysis and comparative study for negative-index metamaterials have been provided by Tassin et al.[294]

8.4. Epsilon-Near-Zero Applications

Epsilon-near-zero applications require that the permittivity of the material approaches zero. Bulk ENZ materials are useful as insulators in nano-optical circuits, in spatial filtering resulting in beaming, and in photon funnels.[129,295,296] A bulk ENZ

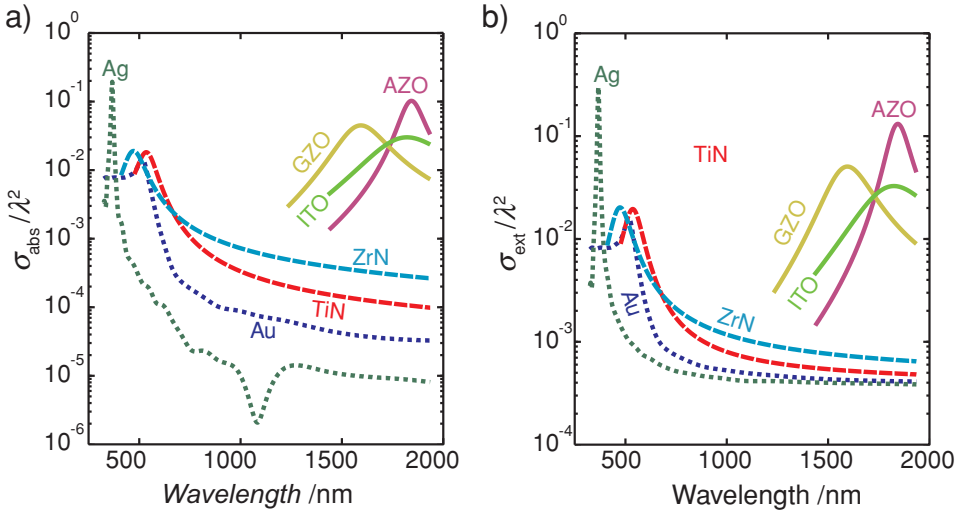

Figure 21. Normalized absorption cross-section (σ_{abs}) and extinction cross-sections (σ_{ext}) of spherical nanospheres of different plasmonic materials. The diameter of the nanospheres is assumed to be a tenth of the wavelength. The nanospheres are assumed to be in a host of refractive index 1.33. The calculations are based on quasistatic approximation.

material requires that both the real and imaginary parts of the permittivity must vanish. However, real materials are always associated with losses and never show ENZ-like behavior. All is not lost, however, as there are materials with a vanishing real permittivity and only a small imaginary part of permittivity at the same wavelength. For example, TCOs have a zero crossing in their real permittivity in the NIR and have small losses in the same range, and thus they can be good ENZ materials. On the other hand, metal nitrides have high losses near their zero crossovers due to interband transition losses, and hence they are not good ENZ candidates.

8.5. Hyperbolic Metamaterials

Hyperbolic materials are strongly anisotropic, possessing opposite signs of real permittivity in orthogonal directions.[297,298] Such a material exhibits hyperbolic dispersion and is therefore called a hyperbolic metamaterial.[299] In other words, the constant energy surface of a HMM in the *k*-domain is a hyperboloid which is an open surface. In contrast, the constant frequency surface of an isotropic dielectric is a sphere, and that of an anisotropic dielectric is an ellipsoid, both of which are closed surfaces. An open surface such as hyperboloid gives rise to many interesting properties, such as a very high effective index and a very large photonic density of states.[300,301] Devices such as the hyperlens rely upon HMMs.[302] Hyperbolic dispersion can be engineered through the use of metamaterials. For example, a stack of alternating sub-wavelength thick layers of metal and dielectric produces hyperbolic dispersion in the effective-medium limit.[73] Similarly, subwavelength-thick metal wires embedded in a dielectric host also produce hyperbolic dispersion in the effective-medium limit.[303,304] From a device fabrication and integration perspective, the superlattice (layered) structure of an HMM would be favorable. In this section, we consider various candidates as the plasmonic element in a layered HMM design. The performance of these HMMs can be compared directly by using a figure of merit (FoM). Hoffman et al.[73] mention that a good FoM for low-loss HMMs would be $\mathrm{Re}(\beta_\perp)/\mathrm{Im}(\beta_\perp)$, where $\beta_\perp$ is the propagation constant for light in the direction perpendicular to the layers. We plot this quantity in **Figure 22** for various superlattices with metal filling fractions of 50%. The curves are plotted in the wavelength range where hyperbolic dispersion exists. The dielectrics chosen with the plasmonic materials are based on ease of fabrication, and for simplicity, their index is assumed constant. Thus TCOs are paired with ZnO with an index of 2.0; titanium and zirconium nitrides are paired with aluminum nitride (index 1.70); and silver and gold are paired with aluminum oxide (index 1.78). In the visible and NIR ranges, alternative plasmonic materials clearly outperform noble metals. However, this conclusion holds only for HMMs in a planar geometry of HMMs, and alternative plasmonic materials may not outperform noble metals for other geometries.

In imaging applications HMMs can be quite useful, but HMMs are of great interest as well in quantum photonics and thermal engineering applications.[299,305–307] These applications rely upon the enhancement of the photonic density of states (PDOS) brought about by the HMM properties. In reality, the limit on the enhancement of PDOS is imposed by the losses in the constituent materials and the size of the smallest structure used to build the HMM. The latter limit could be pushed higher by sophisticated fabrication techniques. However, the former is a limiting factor given that the losses in plasmonic components are high. Jacob et al. show that the enhancement in PDOS for a HMM depends inversely with the cube on the losses.[308] Therefore, HMMs made from low-loss plasmonic materials are extremely important. Since many alternative plasmonic materials have much smaller losses than noble metals, they can be better substitutes for noble metals in HMM applications. In HMM applications such as thermal radiation engineering and thermophotovolataic applications, where a stable high temperature operation is essential, plasmonic materials such as TiN possessing very high melting point are very promising.[307]

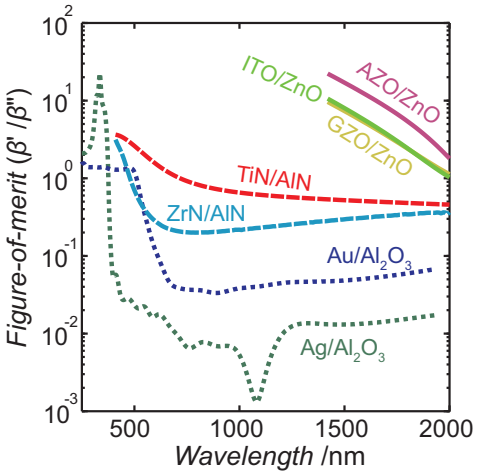

Figure 22. The figure-of-merit of hyperbolic metamaterials (HMMs), as defined in ref.[73] The calculations are for planar alternating layers of metal/dielectric layers formed by different pairs of materials.

8.6. Transformation Optics

Devices and applications that rely on TO often require a specific spatial distribution of permittivity in order to achieve the desired functionality.[7] This is achieved in a composite by varying the fill fraction of one of the constituent elements.[309–311] In the case of those devices that require metals as one of their constituents, the magnitude of real permittivity of the metal should be on the order of that of the dielectric in order to achieve a nearly balanced polarization response in the overall system and create the desired effective parameters. As an example, Cai et al. proposed a non-magnetic cloak using needle-like metallic structures.[28] Such a design is hard to realize using conventional metals because the magnitude of their real permittivity is at least one order higher than that of any dielectric in the optical range. The large magnitude of real permittivity necessitates a small metal fill fraction, which in turn translates into the fabrication of small nanostructures with noble metals. Very small nanostructures of noble metals are hard to fabricate due the many reasons mentioned previously

Table 3. Summary of comparative study of various alternative plasmonic materials for different metamaterial and plasmonic applications in the visible and NIR ranges. ✓ represents suitable; × represents not suitable.

	LSPR	SPPs & Waveguides	NIMs	TO	ENZ	Switchable MMs
Noble Metals	✓	✓	✓	×	×	×
Metal Nitrides	×	✓	×	✓	×	×
TCOs	✓	×	×	✓	✓	✓
Noble Alkali Alloys	×	×	×	✓	✓	×
Alkali Metals	✓	✓	✓	×	×	×
Other Metals	×	×	×	×	×	×
Graphene[a)]	✓	✓	×	✓	×	✓
Conventional semiconductors[a)]	✓	×	×	✓	✓	✓

[a)]Current considerations are only in the mid-IR.

in this review. This issue is alleviated by the use of alternative plasmonic materials because their real permittivity is small in magnitude. Thus, many TO devices could benefit significantly from alternative plasmonic materials.

8.7. Tunable Devices

Tunable devices are technologically important because there are many applications that demand tunablity or ability to dynamically modulate the device characteristics.[9,312,313] Plasmonic and metamaterial devices can be effectively tuned if their plasmonic component is tunable.[314,315] Since the field penetration in a plasmonic material is typically small, tuning a small plasmonic structure could tune the properties of the device quite dramatically. However, noble metals cannot be significantly tuned, and only with difficulty.[187,315–317] On the other hand, some of the alternative plasmonic materials can be tuned rather easily: for example, TCOs can be tuned by the application of an electric field;[175,176] VO_2 may be tuned by inducing a phase change in the material.[181] Therefore, for applications where tuning is required, the benefits of using alternative plasmonic materials are significant.

2D materials such as graphene and semiconductor heterostructures are very useful plasmonic materials owing to their ability to change optical properties by chemical, electrochemical and electrical means.[131,132,252,253,256,261,264,266]

8.8. Summary

Broadly, plasmonics and metamaterial applications can be classified into resonant and non-resonant applications. Resonant devices can be defined as those devices whose operation is based on a localized plasmon resonance in metal-dielectric structures. Hence an LSPR device is resonant, whereas a plasmonic waveguide is non-resonant according to our definition. Superlenses and NIMs are resonant devices, whereas HMMs and TO devices such as cloaks are non-resonant devices. This definition helps us to separate applications into groups with based on how their performance depends on the material properties. In general, alternative plasmonic materials outperform noble metals for non-resonant applications. For resonant device applications, however, noble metals perform better except in the case of applications that leverage the special properties of alternative plasmonic materials. For example, TCO-based plasmonic gas sensors are useful because TCOs are both plasmonic and chemically sensitive to gas, and LSPR modes in spherical nanoparticles also benefit from alternative plasmonic materials because they enable LSPR at longer wavelengths. **Table 3** qualitatively summarizes the discussion on the comparative study of materials for various plasmonic and metamaterial applications. We note that there is no single material that is good for all applications and for all wavelength ranges. However, there are plasmonic materials that are better than noble metals for many metamaterial and plasmonic applications in the visible and NIR ranges.

9. Conclusions and Future Directions

Conventional materials such as gold and silver limit the performance of plasmonic and metamaterial devices in the optical range. For such devices to become integrated into realistic consumer applications, a new material platform must be investigated. To determine the requirements of this new material, a systematic study of the ideal plasmonic material was conducted. Properties including low loss, adjustable carrier concentration, ease of fabrication and integration, chemical stability, tunable optical properties, and CMOS compatibility were important requirements of this new material. While there are many suitable candidates, the best replacement is likely to be dependent on the wavelength of interest. Conventional semiconductors and 2D materials such as graphene would be suitable for mid-IR applications, while TCOs and metal-nitrides will bring significant advances to devices in the NIR and visible ranges. These alternative plasmonic materials were evaluated for their suitability in several applications, and their performance was compared to that of conventional gold and silver. Simply put, there is no single material that offers superior performance for all applications in a given wavelength range. However, the optimization of alternative materials based on wavelength

range has led to devices which outperform conventional gold and silver in many applications. Similar to the way silicon revolutionized the microelectronics industry, the development of better materials will usher in the next-generation of nanophotonic and metamaterial technologies.

Owing to its huge technological impact, materials research for plasmonics and metamaterials is attracting the attention of many researchers. The research in this direction is fairly open-ended, and provides an excellent opportunity to explore and develop new dimensions. Some of the important directions in this field of materials research for plasmonics and metamaterials are listed here:

- Computational and theoretical studies in predicting improved plasmonic materials or materials enabling new functionalities
- Investigation of plasmonic properties of two-dimensional materials such as graphene
- Realization of plasmonic and metamaterial devices with alternative plasmonic materials for improved performance and new functionalities
- Exploration of new physics enabled by alternative plasmonic materials, e.g. ENZ structures, high-performance HMM devices and non-linear plasmonic devices
- Realization of novel classes of active and tunable devices based on new plasmonic materials
- New device concepts enabled by alternative materials, e.g. in sensing, imaging, light generation and harvesting
- Process development for deposition, patterning and integrating new materials into complex plasmonic and metamaterial device geometries
- Reliability and scalability studies for device manufacturing

The development of materials technology, both for plasmonic and dielectric materials, holds the key in transforming the science of plasmonics and metamaterials into a technology of daily use.

Acknowledgements

We thank Prof. Jeorg Appenzeller, Prof. Timothy D. Sands, Prof. N. Engheta, Prof. A. Alu for helpful discussions. We are grateful to Dr. Mark D. Thoreson for helping us in preparing this manuscript. We thank Jongbum Kim, Jingjing Liu, Naresh K. Emani, and Paul R. West for their useful suggestions. We acknowledge support from following grants: ONR-MURI grant N00014-10-1-0942, ARO grant 57981-PH (W911NF-11-1-0359), NSF grant DMR-1120923 and NSF-PREM grant DMR-0611430.

Received: December 9, 2012
Revised: February 19, 2013
Published online: May 15, 2013

[1] G. E. Moore, *Electronics* **1965**, *38*, 4.
[2] R. R. Schaller, *Spectrum, IEEE* **1997**, *34*, 52.
[3] M. Lundstrom, *Science* **2003**, *299*, 210.
[4] M. L. Brongersma, V. M. Shalaev, *Science* **2010**, *328*, 440.
[5] D. Smith, J. Pendry, M. Wiltshire, *Science* **2004**, *305*, 788.
[6] W. Cai, V. Shalaev, *Optical Metamaterials: Fundamentals and Applications*, Springer Verlag, NY, USA **2009**.
[7] J. B. Pendry, D. Schurig, D. R. Smith, *Science* **2006**, *312*, 1780.
[8] A. Boltasseva, H. A. Atwater, *Science* **2011**, *331*, 290.
[9] N. I. Zheludev, *Opt. Photonics News* **2011**, *22*, 30.
[10] N. I. Zheludev, Y. S. Kivshar, *Nat. Mater.* **2012**, *11*, 917.
[11] W. L. Barnes, A. Dereux, T. W. Ebbesen, *Nature* **2003**, *424*, 824.
[12] H. A. Atwater, *Scientific American* **2007**, *296*, 56.
[13] E. Ozbay, *Science* **2006**, *311*, 189.
[14] J. A. Schuller, E. S. Barnard, W. Cai, Y. C. Jun, J. S. White, M. L. Brongersma, *Nat. Mater.* **2010**, *9*, 193.
[15] S. A. Maier, *Plasmonics: Fundamentals and Applications*, Springer Verlag, NY, USA **2007**.
[16] S. Lal, S. Link, N. J. Halas, *Nat. Photonics* **2007**, *1*, 641.
[17] U. Leonhardt, *Science* **2006**, *312*, 1777.
[18] A. V. Kildishev, V. M. Shalaev, *Opt. Lett.* **2008**, *33*, 43.
[19] A. Sihvola, *Metamaterials* **2007**, *1*, 2.
[20] L. Landau, E. Lifshits, *Electrodynamics of Solid Media*, Nauka, Moscow, Russia **1982**.
[21] E. D. Palik, *Handbook of Optical Constants,* Academic Press, San Diego, CA, USA **1985** .
[22] P. B. Johnson, R. Christy, *Phys. Rev. B* **1972**, *6*, 4370.
[23] J. B. Khurgin, A. Boltasseva, *MRS Bull.* **2012**, *37*, 768.
[24] P. R. West, S. Ishii, G. V. Naik, N. K. Emani, V. M. Shalaev, A. Boltasseva, *Laser Photonics Rev.* **2010**, *4*, 795.
[25] P. Drude, *Ann. Phys.* **1900**, *306*, 566.
[26] N. W. Ashcroft, N. D. Mermin, *Solid State Physics*, Saunders College, Philadelphia, PA, USA **1976**.
[27] J. S. G. Bouillard, W. Dickson, D. P. O'Connor, G. A. Wurtz, A. Zayats, *Nano Lett.* **2012**.
[28] W. Cai, U. K. Chettiar, A. V. Kildishev, V. M. Shalaev, *Nat. Photonics* **2007**, *1*, 224.
[29] R. Cohen, G. Cody, M. Coutts, B. Abeles, *Phys. Rev. B* **1973**, *8*, 3689.
[30] Y. Yagil, G. Deutscher, *Thin Solid Films* **1987**, *152*, 465.
[31] F. Abelès, Y. Borensztein, T. López-Rios, *Advances in Solid State Physics*, Vol. *24* (Ed: P. Grosse), Springer Berlin/Heidelberg Germany **1984**.
[32] O. Heavens, *Rep. Prog. Phys.* **1960**, *23*, 1.
[33] L. Kazmerski, D. M. Racine, *J. Appl. Phys.* **1975**, *46*, 791.
[34] P. Clegg, *The Optical Constants of Thin Metallic Films Deposition by Evaporation*, *Proc. Phys. Soc., London, Sect. B* **1952**, *65*, 774.
[35] A. Denier van derGon, R. Tromp, M. Reuter, *Thin Solid Films* **1993**, *236*, 140.
[36] K. H. Park, J. S. Ha, E. H. Lee, *ETRI J.* **1997**, *19*, 71.
[37] V. Logeeswaran, M. L. Chan, Y. Bayam, M. Saif Islam, D. Horsley, X. Li, W. Wu, S. Wang, R. Williams, *Appl. Phys. A: Mater. Sci. Process.* **2007**, *87*, 187.
[38] W. Chen, M. D. Thoreson, S. Ishii, A. V. Kildishev, V. M. Shalaev, *Opt. Express* **2010**, *18*, 5124.
[39] D. Pashley, *Philos. Mag.* **1959**, *4*, 316.
[40] P. Palmberg, T. Rhodin, C. Todd, *Appl. Phys. Lett.* **1967**, *11*, 33.
[41] K. Fuchs, *Math. Proc. Cambridge Philos. Soc.* **1938**, *34*, 100.
[42] F. Warkusz, *Prog. Surf. Sci.* **1980**, *10*, 287.
[43] W. Kraus, G. C. Schatz, *J. Chem. Phys.* **1983**, *79*, 6130.
[44] H. Hövel, S. Fritz, A. Hilger, U. Kreibig, M. Vollmer, *Phys. Rev. B* **1993**, *48*, 18178.
[45] V. P. Drachev, U. K. Chettiar, A. V. Kildishev, H. K. Yuan, W. Cai, V. M. Shalaev, *Opt. Express* **2008**, *16*, 1186.
[46] J. H. Park, P. Ambwani, M. Manno, N. C. Lindquist, P. Nagpal, S. H. Oh, C. Leighton, D. J. Norris, *Adv. Mater.* **2012**, *24*, 3988.
[47] V. Fedotov, T. Uchino, J. Ou, *Opt. Express* **2012**, *20*, 9545.
[48] E. Kretschmann, *Opt. Commun.* **1972**, *6*, 185.
[49] D. L. Hornauer, *Opt. Commun.* **1976**, *16*, 76.
[50] W. Campbell, U. Thomas, *Nature* **1938**, *142*, 253.
[51] G. H. Chan, J. Zhao, E. M. Hicks, G. C. Schatz, R. P. Van Duyne, *Nano Lett.* **2007**, *7*, 1947.

[52] H. Bennett, R. Peck, D. Burge, J. Bennett, *J. Appl. Phys.* **1969**, *40*, 3351.
[53] D. Burge, J. Bennett, R. Peck, H. Bennett, *Surf. Sci.* **1969**, *16*, 303.
[54] H. Jaeger, P. Mercer, R. Sherwood, *Surf. Sci.* **1969**, *13*, 349.
[55] G. Bemski, *Phys. Rev.* **1958**, *111*, 1515.
[56] C. Collins, R. Carlson, *Phys. Rev.* **1957**, *108*, 1409.
[57] L. D. Yau, C. T. Sah, *Appl. Phys. Lett.* **1972**, *21*, 157.
[58] R. J. Gutmann, T. Paul Chow, W. N. Gill, A. E. Kaloyeros, W. A. Lanford, S. P. Murarka, *MRS Proc.* **1994**, 337.
[59] S. Tyagi, M. Alavi, R. Bigwood, T. Bramblett, J. Brandenburg, W. Chen, B. Crew, M. Hussein, P. Jacob, C. Kenyon, presented at *Electron Devices Meeting*, San Francisco, CA, USA, December 2000.
[60] M. G. Blaber, M. D. Arnold, M. J. Ford, *J. Phys. Chem. C* **2009**, *113*, 3041.
[61] M. Blaber, M. Arnold, M. Ford, *J. Phys.: Condens. Matter* **2009**, *21*, 144211.
[62] M. Dressel, G. Grüner, G. F. Bertsch, *Am. J. Phys.* **2002**, *70*, 1269.
[63] J. Khurgin, G. Sun, *Appl. Phys. Lett.* **2010**, 96, 181102.
[64] D. J. Bergman, M. I. Stockman, *Phys. Rev. Lett.* **2003**, *90*, 27402.
[65] R. F. Oulton, V. J. Sorger, D. A. Genov, D. F. P. Pile, X. Zhang, *Nat. Photonics* **2008**, *2*, 496.
[66] M. Noginov, G. Zhu, A. Belgrave, R. Bakker, V. Shalaev, E. Narimanov, S. Stout, E. Herz, T. Suteewong, U. Wiesner, *Nature* **2009**, *460*, 1110.
[67] I. De Leon, P. Berini, *Nat. Photonics* **2010**, *4*, 382.
[68] M. C. Gather, K. Meerholz, N. Danz, K. Leosson, *Nat. Photonics* **2010**, *4*, 457.
[69] S. Xiao, V. P. Drachev, A. V. Kildishev, X. Ni, U. K. Chettiar, H. K. Yuan, V. M. Shalaev, *Nature* **2010**, *466*, 735.
[70] M. Ricci, N. Orloff, S. M. Anlage, *Appl. Phys. Lett.* **2005**, *87*, 034102.
[71] M. C. Ricci, H. Xu, R. Prozorov, A. P. Zhuravel, A. V. Ustinov, S. M. Anlage, *IEEE Trans. Appl. Supercond.* **2007**, *17*, 918.
[72] V. Fedotov, A. Tsiatmas, J. Shi, R. Buckingham, P. de Groot, Y. Chen, S. Wang, N. Zheludev, *Opt. Express* **2010**, *18*, 9015.
[73] A. J. Hoffman, L. Alekseyev, S. S. Howard, K. J. Franz, D. Wasserman, V. A. Podolskiy, E. E. Narimanov, D. L. Sivco, C. Gmachl, *Nat. Mater.* **2007**, *6*, 946.
[74] G. V. Naik, A. Boltasseva, *Phys. Status Solidi RRL* **2010**, *4*, 295.
[75] M. G. Blaber, M. D. Arnold, M. J. Ford, *J. Phys.: Condens. Matter* **2010**, *22*, 143201.
[76] G. V. Naik, J. Kim, A. Boltasseva, *Opt. Mater. Express* **2011**, *1*, 1090.
[77] G. Zgu, E. Narimanov, H. Li, Y. A. Barnakov, M. Noginov, presented at *Frontiers in Optics*, San Jose, CA, USA, October 2009.
[78] G. Zhu, L. Gu, J. Kitur, A. Urbas, J. Vella, M. Noginov, presented at *Quantum Electronics and Laser Science Conf.*, Baltimore, MD, USA, May 2011.
[79] S. E. Harris, *Phys. Today* **1997**, *50*, 36.
[80] K. J. Boller, A. Imamolu, S. Harris, *Phys. Rev. Lett.* **1991**, *66*, 2593.
[81] B. S. Ham, M. S. Shahriar, P. R. Hemmer, *Opt. Lett.* **1997**, *22*, 1138.
[82] Y. Zhao, C. Wu, B.-S. Ham, M. K. Kim, E. Awad, *Phys. Rev. Lett.* **1997**, *79*, 641.
[83] R. Mansfield, *Impurity Scattering in Semiconductors*, *Proc. Phys. Soc., London, Sect. B* **1956**, *69*, 76.
[84] R. B. Fair, *Impurity Doping Processes in Dilicon*, Vol. *2*, (Ed: F. F. Y. Wang) North Holland, New York, NY, USA **1981**.
[85] C. Wolfe, G. Stillman, *Appl. Phys. Lett.* **1975**, *27*, 564.
[86] G. Martin, J. Farges, G. Jacob, J. Hallais, G. Poiblaud, *J. Appl. Phys.* **1980**, *51*, 2840.
[87] F. Trumbore, *Bell Syst. Tech. J* **1960**, *39*, 205.
[88] R. Malik, J. Nagle, M. Micovic, T. Harris, R. Ryan, L. Hopkins, *J. Vac. Sci. Technol., B: Microelectron. Nanometer Struct. – Process. Meas. Phenom.* **1992**, *10*, 850.
[89] M. Yoon, S. Lee, H. Park, H. Kim, M. Jang, *J. Mater. Sci. Lett.* **2002**, *21*, 1703.
[90] R. Soref, *IEEE J. Sel. Top. Quantum Electron.* **2006**, *12*, 1678.
[91] J. A. Dionne, L. A. Sweatlock, M. T. Sheldon, A. P. Alivisatos, H. A. Atwater, *IEEE J. Sel. Top. Quantum Electron.* **2010**, *16*, 295.
[92] A. Hryciw, Y. C. Jun, M. L. Brongersma, *Nat. Mater.* **2010**, *9*, 3.
[93] R. Soref, *Nat. Photonics* **2010**, *4*, 495.
[94] H. Barber, *Solid-State Electron.* **1967**, *10*, 1039.
[95] E. Kooi, *J. Electrochem. Soc.* **1964**, *111*, 1383.
[96] S. Maekawa, *J. Phys. Soc. Jpn.* **1962**, *17*, 1592.
[97] J. Cleary, R. Peale, D. Shelton, G. Boreman, C. Smith, M. Ishigami, R. Soref, A. Drehman, W. Buchwald, *J. Opt. Soc. Am. B* **2010**, *27*, 730.
[98] R. Soref, R. E. Peale, W. Buchwald, J. W. Cleary, presented at *Plasmonics and Metamaterials*, Rochester, NY, USA October 2008.
[99] R. E. Peale, J. W. Cleary, W. R. Buchwald, O. Edwards, presented at *Biomedical Optics*, Miami, FL, USA **2010**.
[100] Y. Takamura, S. Jain, P. Griffin, J. Plummer, *J. Appl. Phys.* **2002**, *92*, 230.
[101] J. R. Haynes, W. Shockley, *Phys. Rev.* **1951**, *81*, 835.
[102] L. Colace, G. Masini, G. Assanto, *IEEE J. Quantum Electron.* **1999**, *35*, 1843.
[103] O. Fidaner, A. K. Okyay, J. E. Roth, R. K. Schaevitz, Y. H. Kuo, K. C. Saraswat, J. S. Harris, D. A. B. Miller, *IEEE Photonics Technol. Lett.* **2007**, *19*, 1631.
[104] J. Michel, J. Liu, L. C. Kimerling, *Nat. Photonics* **2010**, *4*, 527.
[105] S. Assefa, F. Xia, Y. A. Vlasov, *Nature* **2010**, *464*, 80.
[106] E. D. Palik, *Handbook of Optical Constants of Solids*, Academic Press, New York **1985**.
[107] E. D. Palik, *Handbook of Optical Constants of Solids II*, Academic Press/Harcourt Brace, Boston, MA, USA, **1991**.
[108] R. A. Soref, *Proc. IEEE* **1993**, *81*, 1687.
[109] R. Soref, J. Hendrickson, J. W. Cleary, *Opt. Express* **2012**, *20*, 3814.
[110] B. G. Bosch, *Proc. IEEE* **1979**, *67*, 340.
[111] M. Abe, T. Mimura, presented at *12th Annual Gallium Arsenide Integrated Circuit (GaAs IC) Symp. Technical Dig.* **1990**, New Orleans, LA, USA October 1990.
[112] J. Zolper, *Solid-State Electron.* **1998**, *42*, 2153.
[113] B. J. Baliga, *IEEE Electron Device Lett.* **1989**, *10*, 455.
[114] R. F. Davis, *Proc. IEEE* **1991**, *79*, 702.
[115] M. Razeghi, *IEEE J. Sel. Top. Quantum Electron.* **2000**, *6*, 1344.
[116] J. Faist, F. Capasso, D. L. Sivco, C. Sirtori, A. L. Hutchinson, A. Y. Cho, *Science* **1994**, *264*, 553.
[117] B. S. Williams, *Nat. Photonics* **2007**, *1*, 517.
[118] R. E. Nahory, M. A. Pollack, J. W. D. Johnston, R. L. Barns, *Appl. Phys. Lett.* **1978**, *33*, 659.
[119] C. Williams, T. Glisson, J. Hauser, M. Littlejohn, *J. Electron. Mater.* **1978**, *7*, 639.
[120] T. Glisson, J. Hauser, M. Littlejohn, C. Williams, *J. Electron. Mater.* **1978**, *7*, 1.
[121] M. A. Afromowitz, *Solid State Commun.* **1974**, *15*, 59.
[122] B. Broberg, S. Lindgren, *J. Appl. Phys.* **1984**, *55*, 3376.
[123] W. Walukiewicz, J. Lagowski, L. Jastrzebski, P. Rava, M. Lichtensteiger, C. H. Gatos, H. C. Gatos, *J. Appl. Phys.* **1980**, *51*, 2659.
[124] W. Walukiewicz, L. Lagowski, L. Jastrzebski, M. Lichtensteiger, H. C. Gatos, *J. Appl. Phys.* **1979**, *50*, 899.
[125] W. Walukiewicz, *Phys. B: Condens. Matter* **2001**, *302–303*, 123.
[126] J. Neave, P. Dobson, J. Harris, P. Dawson, B. Joyce, *Appl. Phys. A: Mater. Sci. Process.* **1983**, *32*, 195.
[127] T. Yamada, E. Tokumitsu, K. Saito, T. Akatsuka, M. Miyauchi, M. Konagai, K. Takahashi, *J. Cryst. Growth* **1989**, *95*, 145.
[128] S. Law, D. C. Adams, A. M. Taylor, D. Wasserman, *Opt. Express* **2012**, *20*, 12155.

[129] D. Adams, S. Inampudi, T. Ribaudo, D. Slocum, S. Vangala, N. Kuhta, W. Goodhue, V. Podolskiy, D. Wasserman, *Phys. Rev. Lett.* **2011**, *107*, 133901.
[130] T. Kleine-Ostmann, P. Dawson, K. Pierz, G. Hein, M. Koch, *Appl. Phys. Lett.* **2004**, *84*, 3555.
[131] H. T. Chen, W. J. Padilla, J. M. O. Zide, A. C. Gossard, A. J. Taylor, R. D. Averitt, *Nature* **2006**, *444*, 597.
[132] Y. C. Jun, E. Gonzales, J. L. Reno, E. A. Shaner, A. Gabbay, I. Brener, *Opt. Express* **2012**, *20*, 1903.
[133] E. Shaner, J. Cederberg, D. Wasserman, *Appl. Phys. Lett.* **2007**, *91*, 181110.
[134] B. Monemar, *J. Mater. Sci.: Mater. Electron.* **1999**, *10*, 227.
[135] A. Hangleiter, *MRS Bull.* **2003**, *28*, 350.
[136] A. Kasic, M. Schubert, S. Einfeldt, D. Hommel, T. Tiwald, *Phys. Rev. B* **2000**, *62*, 7365.
[137] J. K. Sheu, G. Chi, *J. Phys.: Condens. Matter* **2002**, *14*, R657.
[138] G. C. Yi, B. W. Wessels, *Appl. Phys. Lett.* **1996**, *69*, 3028.
[139] P. Hageman, W. Schaff, J. Janinski, Z. Liliental-Weber, *J. Cryst. Growth* **2004**, *267*, 123.
[140] T. Minami, *Semicond. Sci. Technol.* **2005**, *20*, S35.
[141] G. J. Exarhos, X. D. Zhou, *Thin Solid Films* **2007**, *515*, 7025.
[142] R. G. Gordon, *MRS Proc.* **1996**, 426.
[143] D. H. Kim, M. R. Park, H. J. Lee, G. H. Lee, *Appl. Surf. Sci.* **2006**, *253*, 409.
[144] J. M. Myoung, W. H. Yoon, D. H. Lee, I. Yun, S. H. Bae, S. Y. Lee, *Jpn. J. Appl. Phys.* **2002**, *41*, 28.
[145] J. Kim, G. V. Naik, N. K. Emani, U. Guler, A. Boltasseva, *IEEE J. Sel. Top. Quantum Electron.* **2013**, DOI: 10.1109/jstqe.2013.2238611.
[146] Z. Yang, S. Han, T. Yang, L. Ye, H. Ma, C. Cheng, *Appl. Surf. Sci.* **2000**, *161*, 279.
[147] S. Fernández, A. Martínez-Steele, J. Gandía, F. Naranjo, *Thin Solid Films* **2009**, *517*, 3152.
[148] A. Frölich, M. Wegener, *Opt. Mater. Express* **2011**, *1*, 883.
[149] K. Santiago, R. Mundle, C. B. Samantaray, M. Bahoura, A. Pradhan, *Opt. Mater. Express* **2012**, *2*, 1743.
[150] T. Jia, W. Wang, F. Long, Z. Fu, H. Wang, Q. Zhang, *J. Phys. Chem. C* **2009**, *113*, 9071.
[151] H. D. Jang, C. M. Seong, H. K. Chang, H. C. Kim, *Curr. Appl. Phys.* **2006**, *6*, 1044.
[152] S. I. Choi, K. M. Nam, B. K. Park, W. S. Seo, J. T. Park, *Chem. Mater.* **2008**, *20*, 2609.
[153] S. Hartner, M. Ali, C. Schulz, M. Winterer, H. Wiggers, *Nanotechnology* **2009**, *20*, 445701.
[154] Z. L. Wang, *Mater. Today* **2004**, *7*, 26.
[155] H. K. Yu, W. J. Dong, G. H. Jung, J.-L. Lee, *ACS Nano* **2011**, *5*, 8026.
[156] Q. Wan, E. N. Dattoli, W. Y. Fung, W. Guo, Y. Chen, X. Pan, W. Lu, *Nano Lett.* **2006**, *6*, 2909.
[157] S. Singh, S. K. Arya, P. Pandey, B. Malhotra, S. Saha, K. Sreenivas, V. Gupta, *Appl. Phys. Lett.* **2007**, *91*, 063901.
[158] C. Lao, Y. Li, C. P. Wong, Z. L. Wang, *Nano Lett.* **2007**, *7*, 1323.
[159] M. Curreli, C. Li, Y. Sun, B. Lei, M. A. Gundersen, M. E. Thompson, C. Zhou, *J. Am. Chem. Soc.* **2005**, *127*, 6922.
[160] M. Kanehara, H. Koike, T. Yoshinaga, T. Teranishi, *J. Am. Chem. Soc.* **2009**, *131*, 17736.
[161] G. Garcia, R. Buonsanti, E. L. Runnerstrom, R. J. Mendelsberg, A. Llordes, A. Anders, T. J. Richardson, D. J. Milliron, *Nano Lett.* **2011**, *11*, 4415.
[162] R. Buonsanti, A. Llordes, S. Aloni, B. A. Helms, D. J. Milliron, *Nano Lett.* **2011**, *11*, 4706.
[163] S. Q. Li, P. Guo, L. Zhang, W. Zhou, T. W. Odom, T. Seideman, J. B. Ketterson, R. P. H. Chang, *ACS Nano* **2011**, *5*, 9161.
[164] G. V. Naik, A. Boltasseva, *Metamaterials* **2011**, *5*, 1.
[165] S. K. Mishra, B. D. Gupta, *Plasmonics* **2012**, *7*, 627.
[166] S. K. Mishra, D. Kumari, B. D. Gupta, *Sens. Actuators, B* **2012**, *171–172*, 976.
[167] S. Franzen, *J. Phys. Chem. C* **2008**, *112*, 6027.
[168] S. Franzen, C. Rhodes, M. Cerruti, R. W. Gerber, M. Losego, J.-P. Maria, D. E. Aspnes, *Opt. Lett.* **2009**, *34*, 2867.
[169] C. Rhodes, M. Cerruti, A. Efremenko, M. Losego, D. Aspnes, J. P. Maria, S. Franzen, *J. Appl. Phys.* **2008**, *103*, 093108.
[170] C. Rhodes, S. Franzen, J. P. Maria, M. Losego, D. N. Leonard, B. Laughlin, G. Duscher, S. Weibel, *J. Appl. Phys.* **2006**, *100*, 054905.
[171] M. Noginov, L. Gu, J. Livenere, G. Zhu, A. Pradhan, R. Mundle, M. Bahoura, Y. A. Barnakov, V. Podolskiy, *Appl. Phys. Lett.* **2011**, 99, 021101.
[172] G. V. Naik, J. Liu, A. V. Kildishev, V. M. Shalaev, A. Boltasseva, *Proc. Natl. Acad. Sci. USA* **2012**, *109*, 8834.
[173] H. Cao, J. Y. Wu, H. C. Ong, J. Y. Dai, R. P. H. Chang, *Appl. Phys. Lett.* **1998**, *73*, 572.
[174] G. Wang, G. T. Kiehne, G. K. L. Wong, J. B. Ketterson, X. Liu, R. P. H. Chang, *Appl. Phys. Lett.* **2002**, *80*, 401.
[175] E. Feigenbaum, K. Diest, H. A. Atwater, *Nano Lett.* **2010**, *10*, 2111.
[176] A. Melikyan, N. Lindenmann, S. Walheim, P. M. Leufke, S. Ulrich, J. Ye, P. Vincze, H. Hahn, T. Schimmel, C. Koos, W. Freude, J. Leuthold, *Opt. Express* **2011**, *19*, 8855.
[177] V. E. Babicheva, A. V. Lavrinenko, presented at *Nanophotonics IV*, Brussels, Belgium, April 2012.
[178] Z. Lu, W. Zhao, K. Shi, *IEEE Photonics J.* **2012**, *4*, 735.
[179] C. N. R. Rao, *Philos. Trans. R. Soc., A* **1998**, *356*, 23.
[180] H. W. Verleur, A. S. Barker Jr., C. N. Berglund, *Phys. Rev.* **1968**, *172*, 788.
[181] M. J. Dicken, K. Aydin, I. M. Pryce, L. A. Sweatlock, E. M. Boyd, S. Walavalkar, J. Ma, H. A. Atwater, *Opt. Express* **2009**, *17*, 18330.
[182] S. C. Kehr, Y. M. Liu, L. W. Martin, P. Yu, M. Gajek, S. Y. Yang, C. H. Yang, M. T. Wenzel, R. Jacob, H. G. von Ribbeck, M. Helm, X. Zhang, L. M. Eng, R. Ramesh, *Nat. Commun.* **2011**, *2*, 249.
[183] J. M. Luther, P. K. Jain, T. Ewers, A. P. Alivisatos, *Nat. Mater.* **2011**, *10*, 361.
[184] K. Manthiram, A. P. Alivisatos, *J. Am. Chem. Soc.* **2012**, *134*, 3995.
[185] L. Wang, C. Clavero, K. Yang, E. Radue, M. T. Simons, I. Novikova, R. A. Lukaszew, *Opt. Express* **2012**, *20*, 8618.
[186] M. Blaber, M. Arnold, M. Ford, *J. Phys.: Condens. Matter* **2010**, *22*, 095501.
[187] D. A. Bobb, G. Zhu, M. Mayy, A. V. Gavrilenko, P. Mead, V. I. Gavrilenko, M. A. Noginov, *Appl. Phys. Lett.* **2009**, 95, 151102.
[188] J. T. Lue, S. J. Mu, I. C. Wu, *Phys. Rev. B* **1987**, *36*, 1657.
[189] S. J. Mu, J. T. LuE, I. Wu, *J. Phys. Chem. Solids* **1988**, *49*, 1389.
[190] K. Mistry, C. Allen, C. Auth, B. Beattie, D. Bergstrom, M. Bost, M. Brazier, M. Buehler, A. Cappellani, R. Chau, presented at *Electron Devices Meeting*, Washington, DC, USA, December 2007.
[191] T. Yamamoto, Y. Yamashita, M. Harada, N. Taoka, K. Ikeda, K. Suzuki, O. Kiso, N. Sugiyama, S. Takagi, presented at *Electron Devices Meeting*, Washington, DC, USA, December 2007.
[192] S. Murarka, *J. Vac. Sci. Technol.* **1980**, *17*, 775.
[193] K. Ahn, S. Basavaiah, *Thin Solid Films* **1984**, *118*, 163.
[194] R. S. Biryukova, O. I. Popova, *Powder Metall. Met. Ceram.* **1984**, *23*, 146.
[195] E. D'anna, G. Leggieri, A. Luches, *Appl. Phys. A: Mater. Sci. Process.* **1988**, *45*, 325.
[196] R. T. Tung, J. Poate, J. Bean, J. Gibson, D. Jacobson, *Thin Solid Films* **1982**, *93*, 77.
[197] R. Tung, J. Gibson, J. Poate, *Appl. Phys. Lett.* **1983**, *42*, 888.
[198] Y. Hsieh, L. Chen, E. Marshall, S. Lau, *Appl. Phys. Lett.* **1987**, *51*, 1588.
[199] H. Sun, Y. Chen, X. Pan, D. Chi, R. Nath, Y. Foo, *Appl. Phys. Lett.* **2005**, *87*, 211909.
[200] V. Carron, P. Besson, F. Pierre, *ECS Trans.* **2007**, *11*, 309.
[201] J. Gambino, E. Colgan, *Mater. Chem. Phys.* **1998**, *52*, 99.

[202] T. Chow, A. Steckl, *J. Electrochem. Soc.* **1984**, *131*, 2325.
[203] F. Nava, K. Tu, O. Thomas, J. Senateur, R. Madar, A. Borghesi, G. Guizzetti, U. Gottlieb, O. Laborde, O. Bisi, *Mater. Sci. Rep.* **1993**, *9*, 141.
[204] R. Soref, R. E. Peale, W. Buchwald, *Opt. Express* **2008**, *16*, 6507.
[205] J. Cleary, R. Peale, D. Shelton, G. Boreman, R. Soref, W. Buchwald, *MRS Proc.* **2008**, *1133*, 1.
[206] D. Migas, L. Miglio, V. Shaposhnikov, V. Borisenko, *Physica Status Solidi B* **2002**, *231*, 171.
[207] D. Migas, L. Miglio, V. Shaposhnikov, V. Borisenko, *Phys. Rev. B* **2003**, *67*, 205203.
[208] D. Migas, V. Shaposhnikov, V. Borisenko, *Phys. Status Solidi B* **2007**, *244*, 2611.
[209] D. McWilliams, D. Lynch, *Phys. Rev.* **1963**, *130*, 2248.
[210] N. Lundberg, M. Oestling, F. d'Heurle, *Appl. Surf. Sci.* **1991**, *53*, 126.
[211] Q. Zhang, C. W. Han, C. Zhu, *J. Electrochem. Soc.* **2007**, *154*, H314.
[212] L. Krusin-Elbaum, M. O. Aboelfotoh, *Appl. Phys. Lett.* **1991**, *58*, 1341.
[213] M. Wittmer, *J. Vac. Sci. Technol., A* **1985**, *3*, 1797.
[214] P. Moon, V. Dubin, S. Johnston, J. Leu, K. Raol, C. Wu, presented at *Electron Devices Meeting,* Washington, DC, USA, December 2003.
[215] R. Chau, S. Datta, M. Doczy, B. Doyle, J. Kavalieros, M. Metz, *IEEE Electron. Device Lett.* **2004**, *25*, 408.
[216] J. Lin, R. Augur, S. Shue, C. Yu, M. Liang, A. Vijayendran, T. Suwwan de Felipe, M. Danek, presented at *Interconnect Technology Conf.* Burlingame, CA, USA, June, 2002.
[217] R. Fix, R. G. Gordon, D. M. Hoffman, *Chem. Mater.* **1993**, *5*, 614.
[218] H. Kim, *J. Vac. Sci. Technol., B: Microelectron. Nanometer Struct. – Process. Meas. Phenom.* **2003**, *21*, 2231.
[219] R. Vispute, V. Talyansky, R. Sharma, S. Choopun, M. Downes, T. Venkatesan, Y. Li, L. Salamanca-Riba, A. Iliadis, K. Jones, *Appl. Surf. Sci.* **1998**, *127*, 431.
[220] H. Spillmann, P. Willmott, M. Morstein, P. Uggowitzer, *Appl. Phys. A: Mater. Sci. Process.* **2001**, *73*, 441.
[221] W. Ensinger, K. Volz, M. Kiuchi, *Surf. Coatings Technol.* **2000**, *128*, 81.
[222] I. Kim, P. N. Kumta, *J. Mater. Chem.* **2003**, *13*, 2028.
[223] K. Weil, P. Kumta, *Mater. Sci. Eng. B* **1996**, *38*, 109.
[224] X. Yang, C. Li, L. Yang, Y. Yan, Y. Qian, *J. Am. Ceram. Soc.* **2003**, *86*, 206.
[225] J. Hu, Q. Lu, K. Tang, S. Yu, Y. Qian, G. Zhou, X. Liu, *J. Am. Ceram. Soc.* **2000**, *83*, 430.
[226] J. Li, L. Gao, J. Sun, Q. Zhang, J. Guo, D. Yan, *J. Am. Ceram. Soc.* **2001**, *84*, 3045.
[227] H. S. Seo, T. Y. Lee, I. Petrov, J. Greene, D. Gall, *J. Appl. Phys.* **2005**, *97*, 083521.
[228] C. S. Shin, D. Gall, P. Desjardins, A. Vailionis, H. Kim, I. Petrov, J. Greene, M. Odén, *Appl. Phys. Lett.* **1999**, *75*, 3808.
[229] K. Inumaru, T. Ohara, S. Yamanaka, *Appl. Surf. Sci.* **2000**, *158*, 375.
[230] M. B. Lee, M. Kawasaki, M. Yoshimoto, M. Kumagai, H. Koinuma, *Jpn. J. Appl. Phys., Part 1* **1994**, *33*, 6308.
[231] G. V. Naik, J. L. Schroeder, X. Ni, A. V. Kildishev, T. D. Sands, A. Boltasseva, *Opt. Mater. Express* **2012**, *2*, 478.
[232] J. Narayan, P. Tiwari, X. Chen, J. Singh, R. Chowdhury, T. Zheleva, *Appl. Phys. Lett.* **1992**, *61*, 1290.
[233] C. Walker, J. Matthew, C. Anderson, N. Brown, *Surf. Sci.* **1998**, *412*, 405.
[234] I. leR Strydom, S. Hofmann, *J. Electron Spectrosc. Relat. Phenom.* **1991**, *56*, 85.
[235] T. Chen, A. Viescas, J. D. Curley, D. J. Phares, H. E. Hall, J. Wang, C. Lin, *Phys. Lett. A* **1993**, *173*, 163.
[236] W. Schubert, R. Shelton, E. Wolf, *Phys. Rev. B* **1981**, *23*, 5097.
[237] G. Soto, J. Dıaz, W. De la Cruz, *Mater. Lett.* **2003**, *57*, 4130.
[238] P. Prieto, F. Yubero, E. Elizalde, J. Sanz, *J. Vac. Sci. Technol., A* **1996**, *14*, 3181.
[239] L. E. Koutsokeras, G. M. Matenoglou, P. Patsalas, *Thin Solid Films* **2013**, *528*, 49.
[240] D. Steinmüller-Nethl, R. Kovacs, E. Gornik, P. Rödhammer, *Thin Solid Films* **1994**, *237*, 277.
[241] A. P. Hibbins, J. R. Sambles, C. R. Lawrence, *J. Mod. Opt.* **1998**, *45*, 2051.
[242] N. C. Chen, W. C. Lien, C. R. Liu, Y. L. Huang, Y. R. Lin, C. Chou, S. Y. Chang, C. W. Ho, *J. Appl. Phys.* **2011**, *109*, 043104.
[243] M. Cortie, J. Giddings, A. Dowd, *Nanotechnology* **2010**, *21*, 115201.
[244] U. Guler, G. Naik, A. Boltasseva, V. Shalaev, A. Kildishev, *Appl. Phys. B: Lasers Opt.* **2012**,*107*, 285.
[245] A. Vakil, N. Engheta, *Science* **2011**, *332*, 1291.
[246] F. H. L. Koppens, D. E. Chang, F. J. García de Abajo, *Nano Lett.* **2011**, *11*, 3370.
[247] S. A. Maier, *Nat. Phys.* **2012**, *8*, 581.
[248] A. Grigorenko, M. Polini, K. Novoselov, *Nat. Photonics* **2012**, *6*, 749.
[249] K. Novoselov, V. Fal, L. Colombo, P. Gellert, M. Schwab, K. Kim, *Nature* **2012**, *490*, 192.
[250] L. Ju, B. Geng, J. Horng, C. Girit, M. Martin, Z. Hao, H. A. Bechtel, X. Liang, A. Zettl, Y. R. Shen, *Nat. Nanotechnol.* **2011**, *6*, 630.
[251] H. Yan, X. Li, B. Chandra, G. Tulevski, Y. Wu, M. Freitag, W. Zhu, P. Avouris, F. Xia, *Nat. Nanotechnol.* **2012**, *7*, 330.
[252] J. Chen, M. Badioli, P. Alonso-González, S. Thongrattanasiri, F. Huth, J. Osmond, M. Spasenović, A. Centeno, A. Pesquera, P. Godignon, *Nature* **2012**.
[253] Z. Fei, A. Rodin, G. Andreev, W. Bao, A. McLeod, M. Wagner, L. Zhang, Z. Zhao, M. Thiemens, G. Dominguez, *Nature* **2012**.
[254] F. Stern, *Phys. Rev. Lett.* **1967**, *18*, 546.
[255] E. H. Hwang, S. Das Sarma, *Phys. Rev. B* **2007**, *75*, 205418.
[256] N. Papasimakis, Z. Luo, Z. X. Shen, F. De Angelis, E. Di Fabrizio, A. E. Nikolaenko, N. I. Zheludev, *Opt. Express* **2010**, *18*, 8353.
[257] W. Knap, F. Teppe, N. Dyakonova, D. Coquillat, J. Łusakowski, *J. Phys.: Condens. Matter* **2008**, *20*, 384205.
[258] J. Mannhart, D. G. Schlom, *Science* **2010**, *327*, 1607.
[259] B. Radisavljevic, A. Radenovic, J. Brivio, V. Giacometti, A. Kis, *Nat. Nanotechnol.* **2011**, *6*, 147.
[260] Z. Fang, Z. Liu, Y. Wang, P. M. Ajayan, P. Nordlander, N. J. Halas, *Nano Lett.* **2012**, *12*, 3808.
[261] M. Liu, X. Yin, E. Ulin-Avila, B. Geng, T. Zentgraf, L. Ju, F. Wang, X. Zhang, *Nature* **2011**, *474*, 64.
[262] A. K. Geim, K. S. Novoselov, *Nat. Mater.* **2007**, *6*, 183.
[263] J. J. Cha, K. J. Koski, Y. Cui, *Phys. Status Solidi RRL* **2013**, *7*, 15.
[264] F. Wang, Y. Zhang, C. Tian, C. Girit, A. Zettl, M. Crommie, Y. R. Shen, *Science* **2008**, *320*, 206.
[265] Y. Zhang, T. T. Tang, C. Girit, Z. Hao, M. C. Martin, A. Zettl, M. F. Crommie, Y. R. Shen, F. Wang, *Nature* **2009**, *459*, 820.
[266] N. K. Emani, T. F. Chung, X. Ni, A. V. Kildishev, Y. P. Chen, A. Boltasseva, *Nano Lett.* **2012**, *12*, 5202.
[267] X. Li, X. Wang, L. Zhang, S. Lee, H. Dai, *Science* **2008**, *319*, 1229.
[268] C. L. Stender, E. C. Greyson, Y. Babayan, T. W. Odom, *Adv. Mater.* **2005**, *17*, 2837.
[269] S. Bae, H. Kim, Y. Lee, X. Xu, J.-S. Park, Y. Zheng, J. Balakrishnan, T. Lei, H. Ri Kim, Y. I. Song, Y.-J. Kim, K. S. Kim, B. Ozyilmaz, J.-H. Ahn, B. H. Hong, S. Iijima, *Nat. Nanotechnol.* **2010**, *5*, 574.
[270] C. Zhi, Y. Bando, C. Tang, H. Kuwahara, D. Golberg, *Adv. Mater.* **2009**, *21*, 2889.
[271] T. N. Theis, *Surf. Sci.* **1980**, *98*, 515.
[272] B. Van Wees, H. Van Houten, C. Beenakker, J. G. Williamson, L. Kouwenhoven, D. Van der Marel, C. Foxon, *Phys. Rev. Lett.* **1988**, *60*, 848.
[273] O. Ambacher, J. Smart, J. Shealy, N. Weimann, K. Chu, M. Murphy, W. Schaff, L. Eastman, R. Dimitrov, L. Wittmer, *J. Appl. Phys.* **1999**, *85*, 3222.

[274] H. Y. Hwang, Y. Iwasa, M. Kawasaki, B. Keimer, N. Nagaosa, Y. Tokura, *Nat. Mater.* **2012**, *11*, 103.
[275] K. Novoselov, A. K. Geim, S. Morozov, D. Jiang, M. I. K. I. V. Grigorieva, S. Dubonos, A. Firsov, *Nature* **2005**, *438*, 197.
[276] M. Osada, T. Sasaki, *J. Mater. Chem.* **2009**, *19*, 2503.
[277] M. S. Kushwaha, *Surf. Sci. Rep.* **2001**, *41*, 1.
[278] M. Jablan, H. Buljan, M. Soljačić, *Phys. Rev. B* **2009**, *80*, 245435.
[279] E. P. Rugeramigabo, T. Nagao, H. Pfnür, *Phys. Rev. B* **2008**, *78*, 155402.
[280] A. Muravjov, D. Veksler, V. Popov, M. Shur, N. Pala, X. Hu, R. Gaska, H. Saxena, R. Peale, presented at *The Eur. Conf. on Lasers and Electro-Optics*, Munich, Germany, June 2009.
[281] M. D. Arnold, M. G. Blaber, *Opt. Express* **2009**, *17*, 3835.
[282] D. K. Gramotnev, S. I. Bozhevolnyi, *Nat. Photonics* **2010**, *4*, 83.
[283] P. Berini, *Opt. Express* **2006**, *14*, 13030.
[284] R. Buckley, P. Berini, *Opt. Express* **2007**, 15, 12174.
[285] L. Novotny, B. Hecht, *Principles of Nano-optics*, Cambridge University Press, Cambridge, UK **2006**.
[286] I. Dion, F. Rouais, L. Trut, C. Baquey, J. R. Monties, P. Havlik, *Biomaterials* **1993**, *14*, 169.
[287] P. Taroni, A. Pifferi, A. Torricelli, D. Comelli, R. Cubeddu, *Photochem. Photobiol. Sci.* **2003**, *2*, 124.
[288] O. Neumann, A. S. Urban, J. Day, S. Lal, P. Nordlander, N. J. Halas, *ACS Nano* **2012**, *7*, 42.
[289] M. Blaber, M. Arnold, N. Harris, M. Ford, M. Cortie, *Phys. B: Condens. Matter* **2007**, *394*, 184.
[290] V. M. Shalaev, *Nat. Photonics* **2007**, *1*, 41.
[291] V. Veselago, *Usp. Fiz. Nauk* **1967**, *92*, 517.
[292] J. B. Pendry, *Phys. Rev. Lett.* **2000**, *85*, 3966.
[293] R. Shelby, D. Smith, S. Schultz, *Science* **2001**, *292*, 77.
[294] P. Tassin, T. Koschny, M. Kafesaki, C. M. Soukoulis, *Nat. Photonics* **2012**, *6*, 259.
[295] M. Silveirinha, N. Engheta, *Phys. Rev. Lett.* **2006**, *97*, 157403.
[296] N. Engheta, *Science* **2007**, *317*, 1698.
[297] D. Smith, D. Schurig, *Phys. Rev. Lett.* **2003**, *90*, 77405.
[298] V. A. Podolskiy, E. E. Narimanov, *Phys. Rev. B* **2005**, 71, 201101.
[299] Z. Jacob, V. M. Shalaev, *Science* **2011**, *334*, 463.
[300] Z. Jacob, L. V. Alekseyev, E. Narimanov, *Opt. Express* **2006**, *14*, 8247.
[301] Z. Jacob, I. I. Smolyaninov, E. E. Narimanov, *Appl. Phys. Lett.* **2012**, 100, 181105.
[302] Z. Liu, H. Lee, Y. Xiong, C. Sun, X. Zhang, *Science* **2007**, *315*, 1686.
[303] J. Yao, Z. Liu, Y. Liu, Y. Wang, C. Sun, G. Bartal, A. M. Stacy, X. Zhang, *Science* **2008**, *321*, 930.
[304] M. Noginov, Y. A. Barnakov, G. Zhu, T. Tumkur, H. Li, E. Narimanov, *Appl. Phys. Lett.* **2009**, 94, 151105.
[305] Y. Guo, C. L. Cortes, S. Molesky, Z. Jacob, *Appl. Phys. Lett.* **2012**, 101, 131106.
[306] E. E. Narimanov, I. I. Smolyaninov, arXiv preprint arXiv:1109.5444 **2011**.
[307] S. Molesky, C. J. Dewalt, Z. Jacob, *Opt. Express* **2013**, *21*, A96.
[308] Z. Jacob, in *PhD Thesis*, Purdue University, West Lafayette, IN,USA **2010**.
[309] J. Valentine, J. Li, T. Zentgraf, G. Bartal, X. Zhang, *Nat. Mater.* **2009**, *8*, 568.
[310] L. H. Gabrielli, J. Cardenas, C. B. Poitras, M. Lipson, *Nat. Photonics* **2009**, *3*, 461.
[311] T. Ergin, N. Stenger, P. Brenner, J. B. Pendry, M. Wegener, *Science* **2010**, *328*, 337.
[312] N. I. Zheludev, *Science* **2010**, *328*, 582.
[313] A. D. Boardman, V. V. Grimalsky, Y. S. Kivshar, S. V. Koshevaya, M. Lapine, N. M. Litchinitser, V. N. Malnev, M. Noginov, Y. G. Rapoport, V. M. Shalaev, *Laser Photonics Rev.* **2011**, *5*, 287.
[314] A. V. Krasavin, N. Zheludev, *Appl. Phys. Lett.* **2004**, *84*, 1416.
[315] K. F. MacDonald, Z. L. Sámson, M. I. Stockman, N. I. Zheludev, *Nat. Photonics* **2008**, *3*, 55.
[316] S. K. Dondapati, M. Ludemann, R. Müller, S. Schwieger, A. Schwemer, B. Händel, D. Kwiatkowski, M. Djiango, E. Runge, T. A. Klar, *Nano Lett.* **2012**, *12*, 1247.
[317] A. T. Fafarman, S.-H. Hong, H. Caglayan, X. Ye, B. T. Diroll, T. Paik, N. Engheta, C. B. Murray, C. R. Kagan, *Nano Lett.* **2012**, *13*, 350.
[318] M. Balkanski, A. Aziza, E. Amzallag, *Physica Status Solidi B* **1969**, *31*, 323.
[319] D. Schroder, R. N. Thomas, J. C. Swartz, *IEEE J. Solid-State Circuits* **1978**, *13*, 180.
[320] G. Backenstoss, *Phys. Rev.* **1957**, *108*, 1416.
[321] G. Kroesen, G. Oehrlein, E. De Frésart, G. Scilla, *Appl. Phys. Lett.* **1992**, *60*, 1351.
[322] J. P. Dismukes, L. Ekstrom, E. F. Steigmeier, I. Kudman, D. S. Beers, *J. Appl. Phys.* **1964**, *35*, 2899.
[323] D. Szmyd, M. Hanna, A. Majerfeld, *J. Appl. Phys.* **1990**, *68*, 2376.
[324] F. Kesamanly, Y. V. Maltsev, D. Nasledov, Y. I. Ukhanov, *Phys. Status Solidi B* **1966**, *13*, K119.
[325] D. Anderson, N. Apsley, P. Davies, P. Giles, *J. Appl. Phys.* **1985**, *58*, 3059.
[326] H. Agura, A. Suzuki, T. Matsushita, T. Aoki, M. Okuda, *Thin Solid Films* **2003**, *445*, 263.
[327] S. M. Park, T. Ikegami, K. Ebihara, *Thin Solid Films* **2006**, *513*, 90.
[328] S. Ray, R. Banerjee, N. Basu, A. Batabyal, A. Barua, *J. Appl. Phys.* **1983**, *54*, 3497.